Jeremy T. Shahan and Shawn W. Walker*

Exact shape derivatives with unfitted finite element methods

https://doi.org/10.1515/jnma-2024-0113
Received August 16, 2024; accepted February 19, 2025; published online August 7, 2025

Abstract: We present an approach to shape optimization problems that uses an unfitted finite element method (FEM). The domain geometry is represented, and optimized, using a (discrete) level set function and we consider objective functionals that are defined over bulk domains. For a discrete objective functional, defined in the unfitted FEM framework, we show that the *exact* discrete shape derivative essentially matches the shape derivative at the continuous level. In other words, our approach has the benefits of both optimize-then-discretize and discretize-then-optimize approaches. Specifically, we establish the shape Fréchet differentiability of discrete (unfitted) bulk shape functionals using both the perturbation of the identity approach and direct perturbation of the level set representation. The latter approach is especially convenient for optimizing with respect to level set functions. Moreover, our Fréchet differentiability results hold for *any* polynomial degree used for the discrete level set representation of the domain. We illustrate our results with some numerical accuracy tests, a simple model (geometric) problem with known exact solution, as well as shape optimization of structural designs.

Keywords: shape derivative; PDE constraint; unfitted finite element method; optimize-then-discretize; discretize-then-optimize

MSC 2010: 65N30; 65N85; 49M41

1 Introduction

Considerable work has been done on shape optimization with the following references giving a good overview [1]–[6]. The main idea is to optimize (e.g. minimize) an objective functional over an admissible set of shapes or domains. Typically, the objective functional depends on the solution of a partial differential equation (PDE) over the domain to be optimized [7], [8], which gives a PDE-constrained, shape optimization problem. A classic example is finding the shape of a rigid body in a fluid flow that has minimum drag (i.e. that minimizes the viscous dissipation in the fluid velocity field around the body) [9]–[12]. Other applications can be found in image processing [13], [14], microswimmers and fluids [15]–[17], and optimal (elastic) structures [18], [19].

For practical applications, one usually uses gradient-based optimization to find optimal shapes; thus, one has to calculate *shape derivatives* to obtain effective descent directions [1]. For the continuous problem, one can derive exact shape derivative formulas provided the domain and PDE-data are sufficiently smooth [20]. But these formulas depend on solutions of PDEs, which are almost never analytically tractable. Moreover, the domain geometry must be represented in a way that can be easily varied for optimization purposes. Hence, for real applications, numerical discretization of the PDE and geometry is necessary to make shape optimization problems tractable. A variety of numerical methods may be used for shape optimization, though finite element methods (FEM) are popular [21] because of their ability to handle complex geometry.

However, using FEMs with conforming meshes for the domain geometry introduces an issue for gradient-based optimization methods. The discrete objective functional now depends on the mesh vertex positions in

***Corresponding author: Shawn W. Walker**, Department of Mathematics, Louisiana State University, Baton Rouge, USA, E-mail: walker@math.lsu.edu
Jeremy T. Shahan, Department of Mathematics, Louisiana State University, Baton Rouge, USA, E-mail: jshaha2@lsu.edu

a non-obvious way [22] and can be complicated to differentiate [23], [24] or requires automatic differentiation [25]. Essentially, the difficulty comes from the fact that perturbing the mesh (geometry) also perturbs the finite element space used for computing the PDE solution. The approach just described is called the *Discretize-then-Optimize* approach.

The alternative approach is called *Optimize-then-Discretize*. In this case, one derives the exact shape derivative formulas at the continuous level, then simply replaces all quantities with their discrete approximation [26]. So, computing the derivative is more straightforward than the other approach. Unfortunately, it suffers from *inconsistent gradients*, i.e. the discrete approximation of the shape derivative is **not** the exact derivative of the discrete objective functional. Hence, a gradient-based optimization method that uses these derivatives may get stuck and not reach a true optimum. In addition, one has to deform the mesh as the domain changes which introduces some challenges, such as avoiding mesh degeneracies and general remeshing of the domain [26]. Despite this, some success is enjoyed by this approach [27], [28], but the issues remain. See [29], [30] for a detailed discussion on the *Optimize-then-Discretize* versus *Discretize-then-Optimize* approaches.

Therefore, we propose an unfitted approach for shape optimization that avoids the above dichotomy. Our method uses discrete level set functions to represent the domain and an unfitted FEM for solving the PDEs. We show that, for bulk shape functionals, the exact, discrete shape derivative in terms of perturbing the domain's discrete level set function can be easily computed and, essentially, matches the continuous formula. Effectively, we take the discretize-then-optimize approach, but show that the optimize-then-discretize approach yields the same formula. Ergo, we gain the benefits of both approaches.

In ref. [31], they consider shape optimization with extended FEM and level sets and apply finite differences (with respect to the level set) to the finite element stiffness matrix and load vector. However, this is a purely discretize-then-optimize approach and the computed shape derivative is not easy to interpret. In ref. [32], they consider shape optimization with multi-meshes and they describe a method of mappings approach that yields a (seemingly) simple discrete shape derivative formula that is discretely consistent. However, they demonstrate that applying their formula to a Poisson problem results in a complicated formula involving many jump terms and special extension terms that are not easy to implement within their FEM framework. They then opt for a Hadamard formulation of the shape derivative, which is the optimize-then-discretize approach and gives gradients that are not consistent.

The closest reference to our work is [33], which derived similar level set shape derivative formulas to ours (c.f. our Theorem 9 to [33, Thm 5.1]). Nevertheless, there are two main differences with our work: (i) we are able to prove Fréchet differentiability of our formulas, whereas [33] only proves Gâteaux differentiability; (ii) we allow for discrete level set functions of arbitrary polynomial degree, but [33] only considers piecewise linear level set functions. We also emphasize that [33] assumes that the zero level set does not pass through any vertices of the mesh, which is related to our Assumption 3. It is notable that [33] also considers boundary functionals, which we do not, however the resulting discrete formulas are much more complicated than the continuous versions.

Some other related works are the following. In ref. [18], they apply cutFEM techniques and level sets to shape optimization of elastic structures, but their formulation is of the optimize-then-discretize type only. In ref. [34], they consider a Bernoulli free boundary problem, which can be posed as a shape optimization problem, and its approximation by cutFEM. Moreover, they *formally* compute discrete shape derivatives in the Gâteaux sense under some smoothness assumptions, including a boundary value correction method, and compare these to using continuous derivative formulas. Numerical experiments show that the various derivative formulas perform similarly with some issues of getting stuck on local minimizers.

Recently in ref. [23], they computed the exact shape and topological derivative of discrete shape functionals, but their analysis was limited to piecewise linear level set functions. Our analysis allows for discrete level sets of arbitrary polynomial degree and yields formulas that are easier to interpret than in ref. [23]. Furthermore, [35], [36] presents theoretical tools for shape optimization of sets defined via intersection.

This paper is organized as follows. Section 2 presents a model problem, shape optimization with linear elasticity as the PDE constraint, to illustrate our shape derivative technique. Next, in Section 3, the discretization of the linear elasticity PDE is introduced along with an unfitted finite element framework and existence and uniqueness is established. Section 4 discusses the shape derivative and establishes the shape Fréchet

differentiability of discrete bulk shape functionals. Moreover, the shape derivative is connected to the level set formulation and allows for *direct* perturbation of the level set function. In Section 5, the full shape optimization algorithm is described within a level set framework that allows for directly updating the level set function. Next, we give numerical results in Section 6 to demonstrate the method followed by some concluding remarks in Section 7.

2 Model problem

We setup a classic example problem to illustrate our unfitted approach to shape optimization.

2.1 Linear elasticity

Let $\Omega \subset \mathbb{R}^d$, for $d = 2$ or 3 with Lipschitz boundary $\partial\Omega \equiv \left(\widehat{\Gamma}_{\mathrm{D}} \cup \Gamma_{\mathrm{D}}\right) \cup \left(\widehat{\Gamma}_{\mathrm{N}} \cup \Gamma_{\mathrm{N}}\right)$, where the partition is disjoint (see Section 3.1 for more details). We denote the outward normal of Ω by $\boldsymbol{\nu}$. We consider the following linear elasticity equations with displacement field $\boldsymbol{u}(\boldsymbol{x})$:

$$-\nabla\cdot\boldsymbol{\sigma} = \boldsymbol{f}, \quad \boldsymbol{\sigma} = 2\mu\epsilon(\nabla\boldsymbol{u}) + \lambda\mathrm{tr}(\epsilon(\nabla\boldsymbol{u}))\mathbf{I} \quad \text{in } \Omega, \quad \boldsymbol{u} = \mathbf{0} \quad \text{on } \widehat{\Gamma}_{\mathrm{D}} \cup \Gamma_{\mathrm{D}}, \quad \boldsymbol{\sigma}\boldsymbol{\nu} = \boldsymbol{g}_{\mathrm{N}} \quad \text{on } \widehat{\Gamma}_{\mathrm{N}} \cup \Gamma_{\mathrm{N}}, \tag{1}$$

where $\epsilon(\nabla\boldsymbol{u}) := \frac{1}{2}(\nabla\boldsymbol{u} + \nabla\boldsymbol{u}^T)$, μ and λ are Lamé parameters, and $\boldsymbol{\sigma}$ is the stress tensor. Additionally, $\boldsymbol{f}$ and $\boldsymbol{g}_{\mathrm{N}}$ are body and surface force densities, respectively. The term $\nabla\cdot\boldsymbol{\sigma}$ denotes taking the row-wise divergence on $\boldsymbol{\sigma}$. An example of a 2-D elastic domain Ω is given in Figure 1. The typical physical example we consider is a cantilever, with zero Dirichlet boundary conditions indicating that the cantilever is anchored along $\widehat{\Gamma}_{\mathrm{D}} \cup \Gamma_{\mathrm{D}}$.

The weak formulation of (1) is as follows. First, define the linear and bilinear forms:

$$\begin{aligned} \chi(\Omega;\boldsymbol{v}) &:= (\boldsymbol{f},\boldsymbol{v})_{\Omega} + (\boldsymbol{g}_{\mathrm{N}},\boldsymbol{v})_{\Gamma_{\mathrm{N}}} \quad \forall\boldsymbol{v}\in H^1(\Omega), \\ a(\Omega;\boldsymbol{u},\boldsymbol{v}) &:= 2\mu\big(\epsilon(\nabla\boldsymbol{u}),\epsilon(\nabla\boldsymbol{v})\big)_{\Omega} + \lambda(\nabla\cdot\boldsymbol{u},\nabla\cdot\boldsymbol{v})_{\Omega} \quad \forall\boldsymbol{u},\boldsymbol{v}\in H^1(\Omega). \end{aligned} \tag{2}$$

Then, we seek the unique solution $\boldsymbol{u} \in V_{\mathrm{D}}(\Omega) := \left\{\boldsymbol{v}\in H^1(\Omega)\colon \boldsymbol{v}|_{\widehat{\Gamma}_{\mathrm{D}}\cup\Gamma_{\mathrm{D}}} = \mathbf{0}\right\}$ such that

$$a(\Omega;\boldsymbol{u},\boldsymbol{v}) = \chi(\Omega;\boldsymbol{v}) \quad \forall\boldsymbol{v}\in V_{\mathrm{D}}(\Omega). \tag{3}$$

We will sometimes denote the solution to (3) by $\boldsymbol{u}(\Omega)$ to emphasize the dependence of the solution on the domain Ω.

2.2 Minimization problem

For any $\boldsymbol{v} \in V_D$, let $J(\Omega;\boldsymbol{v})$ be a shape (cost) functional. Furthermore, let $\mathcal{A}$ be a set of admissible domains that accounts for some boundary constraints, regularity properties, etc., and consider the following minimization problem

$$J(\Omega_{\min},\boldsymbol{u}(\Omega_{\min})) = \min_{\Omega\in\mathcal{A},\ \boldsymbol{u}\in V_{\mathrm{D}}(\Omega)} J(\Omega;\boldsymbol{u}) \text{ subject to } \boldsymbol{u} \text{ uniquely solving (3) on } \Omega. \tag{4}$$

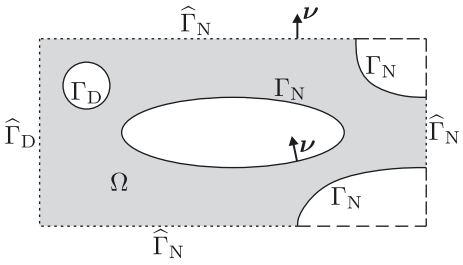

Figure 1: Diagram of the elasticity domain (cantilever) and design domain. The outer design domain boundary $\partial\widehat{\mathfrak{D}}$ is indicated by the long and short dashed line, where the short dashed lines correspond to $\bar{\Omega}\cap\widehat{\Gamma}$; the solid boundaries indicate Γ. The cantilever is anchored on the left and is hanging out freely to the right.

If $\mathcal{A}$ has some compactness properties, such as enforcing a bounded Lipschitz constant on the domains, see ref. [26], then existence of a minimizer can be shown. Note that, ultimately, we are after the derivative of the *reduced functional* $\mathcal{J}(\Omega) := J(\Omega; \boldsymbol{u}(\Omega))$, where $\boldsymbol{u}(\Omega)$ solves (3). Indeed, we seek to compute the shape derivative of $\mathcal{J}(\Omega)$, so that we can perform gradient based optimization (see Section 5.2). As an example shape functional, we take J to be the sum of the so-called *compliance* functional $\chi(\Omega; \boldsymbol{u})$, which is the work of the external forces acting on Ω, plus a penalty term on the volume of the domain:

$$J(\Omega; \boldsymbol{v}) = \chi(\Omega; \boldsymbol{v}) + a_0|\Omega|, \qquad a_0 > 0. \tag{5}$$

Nevertheless, our level set shape derivative formulas can be applied to other bulk shape functionals.

3 Unfitted discretization

Our shape derivative technique takes full advantage of the framework of unfitted FEM, which uses level sets to represent the domain, as well as a Nitsche method and interface stabilization to yield a well-posed problem [37]–[41]. This section describes our discretization of the forward problem (see also [42]).

3.1 Domain representation with level sets

Let $\phi\colon \widehat{\mathfrak{D}} \to \mathbb{R}$ be a C^1 level set function, with $c^{-1} \geqslant |\nabla\phi| \geqslant c > 0$ on $\widehat{\mathfrak{D}}$, where $\widehat{\mathfrak{D}} \subset \mathbb{R}^d$ is a fixed, open, "hold-all," polygonal domain (e.g. a box) that we call the *design domain*. We represent the exact domain by $\Omega = \{\boldsymbol{x} \in \widehat{\mathfrak{D}}\colon \phi(\boldsymbol{x}) < 0\}$ (see Figure 1), where the boundary of Ω partitions as

$$\partial\Omega = \widehat{\Gamma} \cup \Gamma, \qquad \widehat{\Gamma} := \partial\widehat{\mathfrak{D}} \cap \overline{\Omega}, \qquad \Gamma := \{\boldsymbol{x} \in \widehat{\mathfrak{D}}\colon \phi(\boldsymbol{x}) = 0\}, \tag{6}$$

with further partitions of the Dirichlet and Neumann boundaries denoted $\widehat{\Gamma} = \widehat{\Gamma}_{\mathrm{D}} \cup \widehat{\Gamma}_{\mathrm{N}}$, $\Gamma = \Gamma_{\mathrm{D}} \cup \Gamma_{\mathrm{N}}$. Essentially, Γ is the free part of the domain that is being optimized. Note that $\phi \neq 0$ on $\widehat{\Gamma}$, except on $\overline{\widehat{\Gamma}} \cap \overline{\Gamma}$. Thus, we have

$$\partial\Omega \equiv \left(\widehat{\Gamma}_{\mathrm{D}} \cup \Gamma_{\mathrm{D}}\right) \cup \left(\widehat{\Gamma}_{\mathrm{N}} \cup \Gamma_{\mathrm{N}}\right) \equiv \underbrace{\left(\widehat{\Gamma}_{\mathrm{D}} \cup \widehat{\Gamma}_{\mathrm{N}}\right)}_{=\widehat{\Gamma}} \cup \underbrace{\left(\Gamma_{\mathrm{D}} \cup \Gamma_{\mathrm{N}}\right)}_{=\Gamma}, \tag{7}$$

and similarly for the discrete boundaries (see below). The "hatted" boundaries will be *inactive*, while "unhatted" are *active*.

The discrete domain is represented by a discrete version of ϕ, denoted ϕ_h. To this end, let $\widehat{\mathcal{T}}_h = \{T\}$ be a conforming shape regular mesh of $\widehat{\mathfrak{D}}$, where all $T \in \widehat{\mathcal{T}}_h$ are treated as open sets, and define the space

$$\mathcal{B}_h = \left\{\phi_h \in W^{1,\infty}(\widehat{\mathfrak{D}}) \mid \phi_h|_T \in W^{2,\infty}(T) \quad \forall T \in \widehat{\mathcal{T}}_h\right\}, \tag{8}$$

with norm given by

$$\|\phi_h\|_{\mathcal{B}_h} := \|\phi_h\|_{W^{1,\infty}(\widehat{\mathfrak{D}})} + \max_{T\in\widehat{\mathcal{T}}_h} \|\nabla^2\phi_h\|_{L^\infty(T)}. \tag{9}$$

Then, we let $\phi_h \in \mathcal{B}_h$ and define the discrete domain $\Omega_h = \{\boldsymbol{x} \in \widehat{\mathfrak{D}}\colon \phi_h(\boldsymbol{x}) < 0\}$ with

$$\partial\Omega_h = \widehat{\Gamma}_h \cup \Gamma_h, \quad \widehat{\Gamma}_h := \partial\widehat{\mathfrak{D}} \cap \overline{\Omega_h}, \quad \Gamma_h := \{\boldsymbol{x} \in \widehat{\mathfrak{D}}\colon \phi_h(\boldsymbol{x}) = 0\}. \tag{10}$$

Again, we assume $c^{-1} \geqslant |\nabla\phi_h| \geqslant c > 0$ a.e. to guarantee Ω_h is well-defined and $\partial\Omega_h$ has dimension $d-1$. We also have an analogous partitioning of the discrete boundaries as in (7), i.e.

$$\partial\Omega_h \equiv \left(\widehat{\Gamma}_{h,\mathrm{D}} \cup \Gamma_{h,\mathrm{D}}\right) \cup \left(\widehat{\Gamma}_{h,\mathrm{N}} \cup \Gamma_{h,\mathrm{N}}\right) \equiv \left(\widehat{\Gamma}_{h,\mathrm{D}} \cup \widehat{\Gamma}_{h,\mathrm{N}}\right) \cup \left(\Gamma_{h,\mathrm{D}} \cup \Gamma_{h,\mathrm{N}}\right) = \widehat{\Gamma}_h \cup \Gamma_h. \tag{11}$$

In practice, we take $\phi_h \in B_h \subset \mathcal{B}_h$ to be a finite element function where B_h is a fixed, background (Lagrange) finite element space on $\widehat{\mathfrak{D}}$:

$$B_h = \left\{ \boldsymbol{v}_h \in C^0(\widehat{\mathfrak{D}}) : \boldsymbol{v}_h|_T \in \mathcal{P}_k(T), \quad \forall T \in \widehat{\mathcal{T}}_h \right\} \qquad \text{for some } k \geqslant 1. \tag{12}$$

Using level sets to represent geometries has a long history [43], [44], with some recent work on level set functions defined on unstructured meshes [45].

3.2 Subdomains and meshes

For any given domain Ω (an open set with Lipschitz boundary), we approximate it by Ω_h which will be determined from an approximated level set function (as noted in (10)). Note that Ω will be changing due to shape optimization iterations. Let $\delta > 0$ be a layer thickness parameter (to be determined later) for extending domains, i.e. define the open set

$$\Omega_\delta = E_\delta(\Omega) := \left\{ \boldsymbol{x} \in \widehat{\mathfrak{D}} : \operatorname{dist}(\boldsymbol{x}, \Omega) < \delta \right\}, \tag{13}$$

and $\Omega_{h,\delta} = E_\delta(\Omega_h)$. Note that $\Omega_0 \equiv \Omega$ and $\Omega_{h,0} = \Omega_h$. With this, we define the active mesh and corresponding domain (see Figure 2):

$$\mathcal{T}_\delta \equiv \mathcal{T}_{h,\delta}(\Omega_h) = \{ T \in \widehat{\mathcal{T}}_h : \Omega_{h,\delta} \cap T \neq \varnothing \}, \quad \mathfrak{D}_\delta \equiv \mathfrak{D}_{h,\delta}(\Omega_h) = \{ \boldsymbol{x} \in T : T \in \mathcal{T}_{h,\delta}(\Omega_h) \}, \tag{14}$$

where the discrete extended domains $\mathfrak{D}_\delta$ are crude versions (caricatures) of $\Omega_{h,\delta}$.

Next, define the tubular (or shell region) that contains Γ_h (the active part):

$$\Sigma_\delta^\pm \equiv \Sigma_{h,\delta}^\pm(\Gamma_h) = \left\{ \boldsymbol{x} \in \widehat{\mathfrak{D}} : \operatorname{dist}(\boldsymbol{x}, \Gamma_h) \leqslant \delta \right\}, \quad \Sigma_\delta^+ \equiv \Sigma_{h,\delta}^+(\Gamma_h) = \left\{ \boldsymbol{x} \in \widehat{\mathfrak{D}} \setminus \Omega_h : \operatorname{dist}(\boldsymbol{x}, \Gamma_h) \leqslant \delta \right\}, \tag{15}$$

i.e. the shell regions always contain the zero level set. The corresponding meshes are (see Figure 2):

$$\mathcal{T}_{\Sigma^\pm} \equiv \mathcal{T}_{\Sigma_\delta^\pm}(\Gamma_h) = \left\{ T \in \widehat{\mathcal{T}}_h : T \cap \Sigma_\delta^\pm \neq \varnothing \right\}, \quad \mathcal{T}_{\Sigma^+} \equiv \mathcal{T}_{\Sigma_\delta^+}(\Gamma_h) = \left\{ T \in \widehat{\mathcal{T}}_h : T \cap \Sigma_\delta^+ \neq \varnothing \right\}. \tag{16}$$

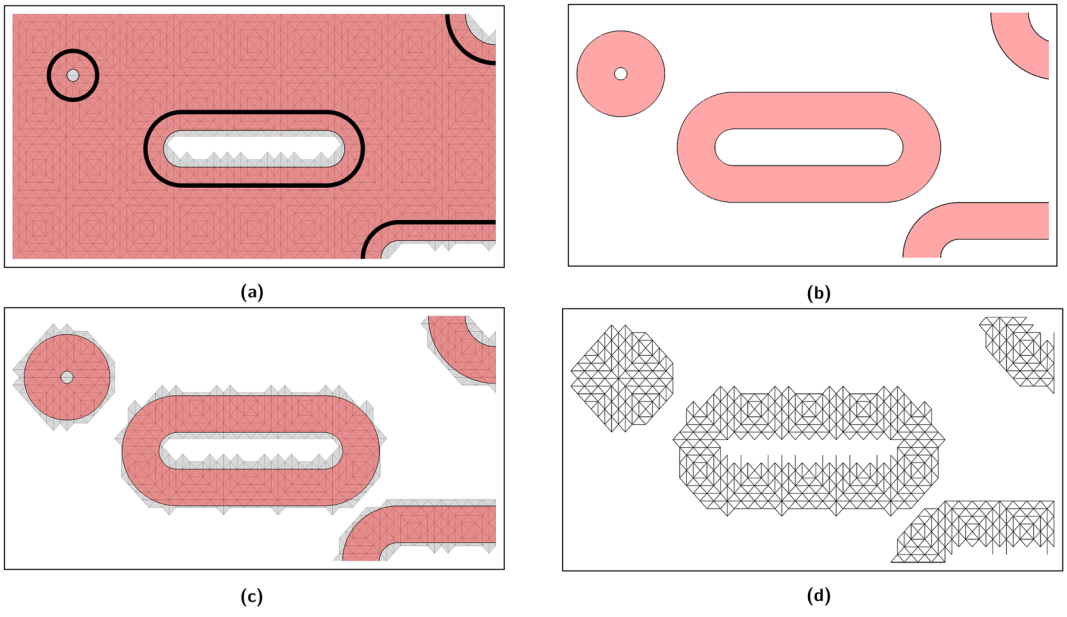

Figure 2: Illustrations of subdomains, meshes, and facets. (a) The active mesh $\mathcal{T}_\delta$ with $\Omega_{h,\delta}$ in red and $\partial\Omega_h$ in thick black. (b) The shell region $\Sigma_\delta^\pm$ is shown in red. (c) The selection of elements, $\mathcal{T}_{\Sigma^\pm}$, around the shell region $\Sigma_\delta^\pm$. (d) The facet selection $\mathcal{F}_{\Sigma^\pm}$ is shown as a collection of edges.

For simplicity, we assume that Γ_{D} and Γ_{N} lie on disconnected parts of Γ so that we have a clear decomposition:

$$\begin{aligned} \Sigma^{\pm}_{h,\delta}(\Gamma_h) = \Sigma^{\pm}_{h,\delta,\mathrm{D}}(\Gamma_{h,\mathrm{D}}) \cup \Sigma^{\pm}_{h,\delta,\mathrm{N}}(\Gamma_{h,\mathrm{N}}), \quad \Sigma^{+}_{h,\delta}(\Gamma_h) = \Sigma^{+}_{h,\delta,\mathrm{D}}(\Gamma_{h,\mathrm{D}}) \cup \Sigma^{+}_{h,\delta,\mathrm{N}}(\Gamma_{h,\mathrm{N}}), \\ \mathcal{T}_{\Sigma^{\pm}_{\delta}}(\Gamma_h) = \mathcal{T}_{\Sigma^{\pm}_{\delta,\mathrm{D}}} \cup \mathcal{T}_{\Sigma^{\pm}_{\delta,\mathrm{N}}}, \quad \mathcal{T}_{\Sigma^{+}_{\delta}}(\Gamma_h) = \mathcal{T}_{\Sigma^{+}_{\delta,\mathrm{D}}} \cup \mathcal{T}_{\Sigma^{+}_{\delta,\mathrm{N}}}. \end{aligned} \tag{17}$$

Letting $\partial\mathcal{T}_{h,\delta}$ be the set of facets of the mesh $\mathcal{T}_{h,\delta}$, we also define the set of shell facets (see Figure 2):

$$\mathcal{F}_{\Sigma^{\pm}} \equiv \mathcal{F}_{\Sigma^{\pm}_{\delta}} = \left\{ F \in \partial\mathcal{T}_{h,\delta} \colon F = \overline{T_1} \cap \overline{T_2} \quad \text{for some } T_1 \in \mathcal{T}_{h,\delta}, T_2 \in \mathcal{T}_{\Sigma^{\pm}}, \text{ such that } T_1 \neq T_2 \right\}, \tag{18}$$

with the following decomposition: $\mathcal{F}_{\Sigma^{\pm}_{\delta}} = \mathcal{F}_{\Sigma^{\pm}_{\delta,\mathrm{D}}} \cup \mathcal{F}_{\Sigma^{\pm}_{\delta,\mathrm{N}}}$. Note that the facets on the boundary of $\mathfrak{D}_{h,\delta}$ are *not* included in (18).

3.3 The finite element scheme

The background finite element space is based on B_h with Dirichlet boundary conditions on $\widehat{\Gamma}_{h,\mathrm{D}}$ built-in:

$$\mathring{B}_h = B_h \cap \left\{ \boldsymbol{v} \in H^1(\widehat{\mathfrak{D}}) \colon \boldsymbol{v}|_{\widehat{\Gamma}_{h,\mathrm{D}}} = 0 \right\}. \tag{19}$$

With this, we have the restricted finite element space on $\mathfrak{D}_{h,\delta}$:

$$V_h \equiv V_h(\Omega_h) = \left\{ \boldsymbol{v}_h \in C^0(\mathfrak{D}_{h,\delta}) \colon \boldsymbol{v}_h = \hat{\boldsymbol{v}}_h|_{\mathfrak{D}_{h,\delta}} \quad \text{for some } \hat{\boldsymbol{v}}_h \in \mathring{B}_h \right\}, \tag{20}$$

i.e. $V_h = \mathring{B}_h|_{\mathfrak{D}_{h,\delta}}$.

The unfitted approach [42] for (3) requires special facet stabilization terms to ensure that the method is stable and that the condition number of the corresponding (finite dimensional) linear system does *not* depend on how elements are cut by the boundary. Given a facet $F = \overline{T_1} \cap \overline{T_2}$, with $T_1 \neq T_2$, let $\omega_F = T_1 \cup T_2$ be the local facet "patch." For any $\boldsymbol{u}, \boldsymbol{v} \in B_h$, define the local stabilization form, known as the "direct" version of the ghost penalty method as in ref. [41]: $s_{h,F}(\boldsymbol{u}, \boldsymbol{v}) := \left(\boldsymbol{u}_1 - \boldsymbol{u}_2, \boldsymbol{v}_1 - \boldsymbol{v}_2\right)_{\omega_F}$, where $\boldsymbol{u}_i = \mathcal{E}_{\mathcal{P}}\left(\boldsymbol{u}|_{T_i}\right)$ $(i = 1, 2)$, and similarly for $\boldsymbol{v}_i$, where $\mathcal{E}_{\mathcal{P}} \colon \mathcal{P}_k(T) \to \mathcal{P}_k(\mathbb{R}^d)$ is the obvious extension of a polynomial on an element T to all of $\mathbb{R}^d$ using its analytic formula. For the analysis, we also define $s_{h,F}(\boldsymbol{u}, \boldsymbol{v})$ for arbitrary functions $\boldsymbol{u}, \boldsymbol{v} \in L^2(\widehat{\mathfrak{D}})$. Set $\boldsymbol{u}_i = \mathcal{E}_{\mathcal{P}}\left(\Pi_{T_i}\boldsymbol{u}|_{T_i}\right)$ $(i = 1, 2)$, where Π_{T_i} is the $L^2(T_i)$ projection onto $\mathcal{P}_k(T_i)$.

The global stabilization form, for a set of facets $\mathcal{F}$, is given by

$$s_h(\mathcal{F}; \boldsymbol{u}, \boldsymbol{v}) := \frac{1}{h^2} \sum_{F \in \mathcal{F}} s_{h,F}(\boldsymbol{u}, \boldsymbol{v}), \tag{21}$$

where $s_h(\mathcal{F}; \boldsymbol{u}, \boldsymbol{v}) \leqslant \left(s_h(\mathcal{F}; \boldsymbol{u}, \boldsymbol{u})\right)^{1/2} \left(s_h(\mathcal{F}; \boldsymbol{v}, \boldsymbol{v})\right)^{1/2}$ follows because $s_h(\mathcal{F}; \cdot, \cdot)$ can be viewed as an inner product. Then, we introduce the following stabilized bilinear form:

$$a_h\left(\Omega_h; \boldsymbol{u}, \boldsymbol{v}\right) := a\left(\Omega_h; \boldsymbol{u}, \boldsymbol{v}\right) + \gamma_{\mathrm{s}} s_h\left(\mathcal{F}_{\Sigma^{\pm}_{\delta,D}}; \boldsymbol{u}, \boldsymbol{v}\right) + \gamma_{\mathrm{s}} h^2 s_h\left(\mathcal{F}_{\Sigma^{\pm}_{\delta,N}}; \boldsymbol{u}, \boldsymbol{v}\right), \tag{22}$$

where $\gamma_{\mathrm{s}} > 0$.

Next, we introduce the Nitsche stabilization technique for handling boundary conditions in our unfitted method. For all $\boldsymbol{u}, \boldsymbol{v} \in B_h$, define the following forms:

$$\begin{aligned} A_h\left(\Omega_h; \boldsymbol{u}, \boldsymbol{v}\right) &:= a_h\left(\Omega_h; \boldsymbol{u}, \boldsymbol{v}\right) - (\boldsymbol{\sigma}(\boldsymbol{u})\boldsymbol{\nu}_h, \boldsymbol{v})_{\Gamma_{h,\mathrm{D}}} - (\boldsymbol{u}, \boldsymbol{\sigma}(\boldsymbol{v})\boldsymbol{\nu}_h)_{\Gamma_{h,\mathrm{D}}} \\ &\quad + \gamma_{\mathrm{D}} h^{-1} b\left(\Omega_h; \boldsymbol{u}, \boldsymbol{v}\right) + \gamma_{\mathrm{N}} h (\boldsymbol{\sigma}(\boldsymbol{u})\boldsymbol{\nu}_h, \boldsymbol{\sigma}(\boldsymbol{v})\boldsymbol{\nu}_h)_{\Gamma_{h,\mathrm{N}}}, \\ b\left(\Omega_h; \boldsymbol{u}, \boldsymbol{v}\right) &:= 2\mu(\boldsymbol{u}, \boldsymbol{v})_{\Gamma_{h,\mathrm{D}}} + \lambda(\boldsymbol{u} \cdot \boldsymbol{\nu}_h, \boldsymbol{v} \cdot \boldsymbol{\nu}_h)_{\Gamma_{h,\mathrm{D}}}, \\ \chi_h\left(\Omega_h; \boldsymbol{v}\right) &:= \chi\left(\Omega_h; \boldsymbol{v}\right) + \gamma_{\mathrm{N}} h (\boldsymbol{g}_{\mathrm{N}}, \boldsymbol{\sigma}(\boldsymbol{v})\boldsymbol{\nu}_h)_{\Gamma_{h,\mathrm{N}}}, \end{aligned} \tag{23}$$

where $\gamma_{\mathrm{D}} > 0, \gamma_{\mathrm{N}} \geqslant 0$ are fixed coefficients. These forms are similarly defined on the exact domain Ω.

Our unfitted numerical scheme is as follows. Find $\boldsymbol{u}_h \in V_h(\Omega_h)$ such that

$$A_h(\Omega_h; \boldsymbol{u}_h, \boldsymbol{v}_h) = \chi_h(\Omega_h; \boldsymbol{v}_h) \quad \forall \boldsymbol{v}_h \in V_h(\Omega_h), \tag{24}$$

where the Dirichlet condition on $\Gamma_{h,\mathrm{D}}$ is only penalized here. This scheme is a slight variation of the unfitted finite element method in ref. [42] (see also ref. [46]).

3.4 Error analysis of the forward problem

We give a brief overview of the error analysis for the approximation of (3) with (24). To this end, we define some convenient norms:

$$\begin{aligned} \|\boldsymbol{v}\|_{a_h}^2 &:= a_h(\Omega_h; \boldsymbol{v}, \boldsymbol{v}), \quad \|\boldsymbol{v}\|_b^2 := b(\Omega_h; \boldsymbol{v}, \boldsymbol{v}), \\ |||\boldsymbol{v}|||_h^2 &:= \|\boldsymbol{v}\|_{a_h}^2 + h\|\boldsymbol{\sigma}(\boldsymbol{v})\|_{L^2(\Gamma_{h,\mathrm{D}})}^2 + \gamma_{\mathrm{N}} h\|\boldsymbol{\sigma}(\boldsymbol{v})\boldsymbol{\nu}_h\|_{L^2(\Gamma_{h,\mathrm{N}})}^2 + h^{-1}\|\boldsymbol{v}\|_b^2 \end{aligned} \tag{25}$$

for all $\boldsymbol{v} \in H^2(\widehat{\mathfrak{D}}) \cup B_h$.

We first note the following coercivity result which can be found in refs. [42], [46] and references therein.

Proposition 1. *The bilinear form A_h is continuous and, for sufficiently large γ_{D}, coercive. Specifically, we have*

$$A_h(\Omega_h; \boldsymbol{u}, \boldsymbol{v}) \lesssim |||\boldsymbol{u}|||_h |||\boldsymbol{v}|||_h \quad \forall\, \boldsymbol{u}, \boldsymbol{v} \in V_h(\Omega_h), \quad |||\boldsymbol{v}|||_h^2 \lesssim A_h(\Omega_h; \boldsymbol{v}, \boldsymbol{v}) \quad \forall\, \boldsymbol{v} \in V_h(\Omega_h).$$

Therefore, by Proposition 1, and since χ_h is a bounded linear functional, there exists a unique solution $\boldsymbol{u}_h \in V_h(\Omega_h)$ of (24) by the Lax-Milgram Theorem. Furthermore, we note that the conditioning of the stiffness matrix corresponding to A_h is well behaved with respect to how the domain Ω_h "cuts" the background mesh $\widehat{\mathcal{T}}_h$ [42].

3.4.1 Pseudo-Galerkin orthogonality

We recall that our bilinear form $A_h(\Omega_h; \boldsymbol{u}, \boldsymbol{v})$ can be defined for functions $\boldsymbol{u}, \boldsymbol{v} \in H^1(\Omega_h)$. Moreover, we can extend the exact solution $\boldsymbol{u}$ on Ω to an open neighborhood $\mathfrak{D}_\delta$ that contains both Ω and Ω_h using the following bounded extension operator (see [47, Thm. 1.4.5]).

Theorem 1. *Suppose that Ω has a Lipschitz boundary and let $v \in W^{k,p}(\Omega)$. Then, there is an extension mapping $E\colon W^{k,p}(\Omega) \to W^{k,p}(\mathbb{R}^d)$ such that for all integers $k \geqslant 0$ and all $1 \leqslant p \leqslant \infty$, that satisfies*

$$E(v)|_\Omega = v \quad \text{and} \quad \|E(v)\|_{W^{k,p}(\mathbb{R}^d)} \leqslant C\|v\|_{W^{k,p}(\Omega)},$$

where C is independent of v.

Now let $\boldsymbol{u} \in H^1(\Omega)$, with $\boldsymbol{u} = \boldsymbol{0}$ on $\Gamma_{\mathrm{D}} \cup \widehat{\Gamma}_{\mathrm{D}}$, solve (1) and assume $\boldsymbol{u} \equiv E(\boldsymbol{u})$ is extended to $H^1(\widehat{\mathfrak{D}})$ using Theorem 1. Then, $\boldsymbol{u}$ satisfies the following:

$$\begin{aligned} (\boldsymbol{f}, \boldsymbol{v})_{\Omega_h} &= -(\nabla \cdot \boldsymbol{\sigma}(\boldsymbol{u}), \boldsymbol{v})_{\Omega_h} = -(\boldsymbol{\sigma}(\boldsymbol{u})\boldsymbol{\nu}_h, \boldsymbol{v})_{\partial\Omega_h} + (\boldsymbol{\sigma}(\boldsymbol{u}), \nabla \boldsymbol{v})_{\Omega_h} \\ &= -(\boldsymbol{\sigma}(\boldsymbol{u})\boldsymbol{\nu}_h, \boldsymbol{v})_{\Gamma_{h,\mathrm{D}}} - (\boldsymbol{g}_{\mathrm{N}}, \boldsymbol{v})_{\Gamma_{h,\mathrm{N}}} + 2\mu(\epsilon(\nabla \boldsymbol{u}), \epsilon(\nabla \boldsymbol{v}))_{\Omega_h} + \lambda(\nabla \cdot \boldsymbol{u}, \nabla \cdot \boldsymbol{v})_{\Omega_h}, \end{aligned} \tag{26}$$

where $\boldsymbol{v} \in \mathring{B}_h$ and $\boldsymbol{v} = \boldsymbol{0}$ on $\widehat{\Gamma}_{h,\mathrm{D}} \equiv \Gamma_{h,\mathrm{D}}$.

The following proposition is used in the error analysis and in the analysis of shape derivatives on "cut" subdomains in Section 4.3.1.

Proposition 2. *Let $\boldsymbol{R}(\boldsymbol{a}, t) := \boldsymbol{a} + tY(\boldsymbol{a})$, for all t in a bounded, open interval I, and a.e. $\boldsymbol{a} \in \mathbb{R}^d$, where $Y \in [W^{1,\infty}(\mathbb{R}^d)]^d$. Assume that $\|Y\|_{W^{1,\infty}}$ is sufficiently small so that for all $t \in I$, $\nabla_{\boldsymbol{a}} \boldsymbol{R}(\boldsymbol{a}, t)$ is a matrix with positive*

determinant and $|\nabla_{\boldsymbol{a}}\boldsymbol{R}(\boldsymbol{a},t)| = O(1)$*, i.e.* $\boldsymbol{R}(\cdot,t):\mathbb{R}^d \to \mathbb{R}^d$ *is a differentiable homeomorphism for all* $t \in I$*. Let* $g \in L^1(\mathbb{R}^d)$ *and define* $q:\mathbb{R}^d \times I \to \mathbb{R}$ *by* $q(\boldsymbol{a},t) = g \circ \boldsymbol{R}(\boldsymbol{a},t)$*. Then,* $q \in L^1(\mathbb{R}^d \times I)$ *and* $\|q\|_{L^1(\mathbb{R}^d\times I)} \leqslant C|I| \cdot \|g\|_{L^1(\mathbb{R}^d)}$ *for some bounded constant* C*.*

Proof. A standard application of measure theory. □

Corollary 1. *Let* $\boldsymbol{R}(\boldsymbol{a},t)$ *have the same function defined in Proposition 2. Now let* $g \in H^1(\mathbb{R}^d)$ *and let* $\Gamma \subset \mathbb{R}^d$ *be the Lipschitz boundary of a bounded set* Ω*, and define* $q:\Gamma \times I \to \mathbb{R}$ *by* $q(\boldsymbol{a},t) = g \circ \boldsymbol{R}(\boldsymbol{a},t)$*. Then,* $q \in L^2(\Gamma \times I)$ *and* $\|q\|_{L^2(\Gamma\times I)} \leqslant C|I|^{1/2}\|g\|_{H^1(\mathbb{R}^d)}$ *for some bounded constant* C*.*

The following assumptions and results are needed to derive the usual error estimates between our finite element solution of (24) and the exact solution of (3). In doing this, we assume that Ω is of class C^{q+1}, with $q \geqslant 1$. For a typical cantilever (see Figure 1), this is not actually true because there are corners. It is possible to have a more refined analysis that allows for piecewise smooth domains, but we do not pursue this here. We emphasize that our discrete shape derivative formulas in Section 4 are not affected by the regularity of the exact solution.

Assumption 1. We assume that the exact domain Ω is of class C^{q+1}, with $q \geqslant 1$, that Ω_h is the sub-zero level set of a discrete level set function ϕ_h having polynomial degree q, and that Ω_h approximates Ω to order q as described in (27) and (28). We also define our finite element space V_h to contain piecewise polynomials of up to order q and assume that $\boldsymbol{g}_{\mathrm{N}} \in H^q(\widehat{\mathfrak{D}})$, $\boldsymbol{f} \in H^{q-1}(\widehat{\mathfrak{D}})$.

Assumption 1 implies that the exact solution has regularity $\boldsymbol{u} \in H^{q+1}(\Omega)$. So, by the extension operator in Theorem 1, we consider $\boldsymbol{u}$ to be extended onto $\widehat{\mathfrak{D}}$ with $\boldsymbol{u} \in H^{q+1}(\widehat{\mathfrak{D}})$.

The error analysis uses the approach in refs. [41], [48] where we have an approximation of the discrete domain Ω_h, with the discrete level set function ϕ_h, satisfying $\operatorname{dist}(\Omega,\ \Omega_h) \lesssim h^{q+1}$, where $q \geqslant 1$ is the order of the geometry approximation (i.e. q is the polynomial degree of ϕ_h). Additionally, we assume that there exists a mapping $\boldsymbol{\Phi}$ with the following properties:

$$\begin{gathered}\boldsymbol{\Phi}(\Omega) = \Omega_h, \qquad \boldsymbol{\Phi}(\Omega_\delta) = \Omega_{h,\delta}, \qquad \|\boldsymbol{\Phi} - \mathbf{id}\|_{L^\infty(\Omega_\delta)} \lesssim h^{q+1}, \\ \|\nabla\boldsymbol{\Phi} - I\|_{L^\infty(\Omega_\delta)} \lesssim h^q, \qquad \|\det(\nabla\boldsymbol{\Phi}) - 1\|_{L^\infty(\Omega_\delta)} \lesssim h^q,\end{gathered} \tag{27}$$

where $\boldsymbol{\Phi}$ is a continuous well-defined map that is invertible for sufficiently small h. In addition, we have

$$\|\boldsymbol{\nu} - \boldsymbol{\nu}_h\|_{L^\infty(\Gamma_h)} \lesssim h^q, \tag{28}$$

where $\boldsymbol{\nu} = \nabla\phi/|\nabla\phi|$ on Γ, $\boldsymbol{\nu}_h = \nabla\phi_h/|\nabla\phi_h|$ on Γ_h. For surface elements, we note the following similar estimate from [48]:

$$dS_h(\boldsymbol{\Phi}(\boldsymbol{a})) = \mu_h dS(\boldsymbol{a}), \quad \|\mu_h - 1\|_{L^\infty(\Gamma_h)} \lesssim h^q, \tag{29}$$

where dS_h (dS) represents the Lebesgue measure for Γ_h (Γ). We abuse notation and use dS for either Γ or Γ_h depending on the context. The function μ_h is the Jacobian resulting from the change of variables for the surface integral.

The following basic result is needed to deal with the boundary stabilization terms coming from Nitsche's method (see Proposition 4).

Proposition 3. *Assume* Ω, Ω_h *satisfy the approximation properties* (27) *and* (29)*. Let* $\Theta \subset \partial\Omega$ *and* Θ_h *be its discrete approximation. Suppose* $f \in H^1(\widehat{\mathfrak{D}})$ *with* $f = 0$ *on* Θ*, and* g_h *is a piecewise polynomial function over* $\widehat{\mathcal{T}}_h$*. Then,*

$$\left(f, g_h\right)_{\Theta_h} \lesssim h^{(q+1)/2}\|f\|_{H^1(\widehat{\mathfrak{D}})} \cdot \|g_h\|_{L^2(\Theta_h)}, \tag{30}$$

$$\left(f, g_h\right)_{\Theta_h} \lesssim h^{q+1}\|\nabla f\|_{H^1(\widehat{\mathfrak{D}})} \cdot \|g_h\|_{L^2(\Theta_h)}, \quad \text{if } f \in H^2(\widehat{\mathfrak{D}}). \tag{31}$$

Proof. We start with

$$\begin{aligned}(f, g_h)_{\Theta_h} &= \int_{\Theta_h} f(x) g_h(x) \mathrm{d}S = \int_{\Theta} (f \circ \boldsymbol{\Phi})(g_h \circ \boldsymbol{\Phi}) \mu_h \mathrm{d}S = \int_{\Theta} (f \circ \boldsymbol{\Phi} - f)(g_h \circ \boldsymbol{\Phi}) \mu_h \mathrm{d}S \\ &\lesssim \int_{\Theta} |(f \circ \boldsymbol{\Phi} - f)(g_h \circ \boldsymbol{\Phi})| \mathrm{d}S \lesssim \|f \circ \boldsymbol{\Phi} - f\|_{L^2(\Theta)} \cdot \|g_h \circ \boldsymbol{\Phi}\|_{L^2(\Theta)},\end{aligned} \tag{32}$$

and note that $\|g_h \circ \boldsymbol{\Phi}\|_{L^2(\Theta)} \cong \|g_h\|_{L^2(\Theta_h)}$. Next, we focus on the f term and use a refined trace estimate:

$$\|f \circ \boldsymbol{\Phi} - f\|^2_{L^2(\Theta)} \leqslant \|f \circ \boldsymbol{\Phi} - f\|^2_{L^2(\partial\Omega)} \lesssim \|f \circ \boldsymbol{\Phi} - f\|_{L^2(\Omega)} \|f \circ \boldsymbol{\Phi} - f\|_{H^1(\Omega)},$$

followed by

$$\begin{aligned}\|f \circ \boldsymbol{\Phi} - f\|_{L^2(\Omega)} &\lesssim \left\| \int_0^1 \nabla f(\mathbf{id} + t(\boldsymbol{\Phi} - \mathbf{id})) \cdot (\boldsymbol{\Phi} - \mathbf{id}) \mathrm{d}t \right\|_{L^2(\Omega)} \\ &\lesssim h^{q+1} \left\| \int_0^1 |\nabla f(\mathbf{id} + t(\boldsymbol{\Phi} - \mathbf{id}))| \mathrm{d}t \right\|_{L^2(\Omega)} \lesssim h^{q+1} \|\nabla f\|_{L^2(\widehat{\mathfrak{D}})},\end{aligned}$$

where we used Proposition 2 to view $\nabla f(\mathbf{id} + t(\boldsymbol{\Phi} - \mathbf{id}))$ as a function in $L^2(\widehat{\mathfrak{D}} \times [0,1])$ and apply the norm bound. Combining everything, we get (30).

Now, assume additional regularity of f, namely $f \in H^2(\Omega)$, and reconsider the f term in (32):

$$\begin{aligned}\|f \circ \boldsymbol{\Phi} - f\|^2_{L^2(\Theta)} &= \left\| \int_0^1 \nabla f(\mathbf{id} + t(\boldsymbol{\Phi} - \mathbf{id})) \cdot (\boldsymbol{\Phi} - \mathbf{id}) \mathrm{d}t \right\|^2_{L^2(\Theta)} \lesssim h^{2(q+1)} \left\| \int_0^1 |\nabla f(\mathbf{id} + t(\boldsymbol{\Phi} - \mathbf{id}))| \mathrm{d}t \right\|^2_{L^2(\Theta)} \\ &\lesssim h^{2(q+1)} \int_{\Theta} \int_0^1 |\nabla f(\mathbf{id} + t(\boldsymbol{\Phi} - \mathbf{id}))|^2 \mathrm{d}t \mathrm{d}S \cong h^{2(q+1)} \|\nabla f \circ \boldsymbol{R}\|^2_{L^2(\Theta \times [0,1])},\end{aligned}$$

where $\boldsymbol{R}(\boldsymbol{a}, t) = \mathbf{id}(\boldsymbol{a}) + t(\boldsymbol{\Phi}(\boldsymbol{a}) - \mathbf{id}(\boldsymbol{a}))$. Then, we apply the trace inequality in Corollary 1 to obtain

$$\|f \circ \boldsymbol{\Phi} - f\|_{L^2(\Theta)} \lesssim h^{q+1} \|\nabla f\|_{H^1(\widehat{\mathfrak{D}})},$$

and combine with (32) to get (31). □

Proposition 4. *Let $q \geqslant 1$ be the order of approximation of Ω_h and assume Ω is C^{q+1}. Moreover, if $q = 1$, assume the (extended) exact solution $\boldsymbol{u}$ is in $H^2(\widehat{\mathfrak{D}})$ and $\boldsymbol{g}_{\mathrm{N}} \in H^1(\widehat{\mathfrak{D}})$; else, $\boldsymbol{u} \in H^3(\widehat{\mathfrak{D}})$ and $\boldsymbol{g}_{\mathrm{N}} \in H^2(\widehat{\mathfrak{D}})$. Then, for all $\boldsymbol{v}_h \in V_h(\Omega_h)$, we have*

$$\begin{aligned}\gamma_{\mathrm{D}} h^{-1} b(\Omega_h; \boldsymbol{u}, \boldsymbol{v}_h) &\lesssim h^q \|\boldsymbol{u}\|_{H^2(\widehat{\mathfrak{D}})} \|\boldsymbol{v}_h\|_{H^1(\Omega_h)}, \\ -(\boldsymbol{u}, \boldsymbol{\sigma}(\boldsymbol{v}_h)\boldsymbol{\nu}_h)_{\Gamma_{h,\mathrm{D}}} &\lesssim h^{q+1/2} \|\boldsymbol{u}\|_{H^2(\widehat{\mathfrak{D}})} |\!|\!| \boldsymbol{v}_h |\!|\!|_h, \\ \gamma_{\mathrm{N}} h (\boldsymbol{\sigma}(\boldsymbol{u})\boldsymbol{\nu}_h - \boldsymbol{g}_{\mathrm{N}}, \boldsymbol{\sigma}(\boldsymbol{v}_h)\boldsymbol{\nu}_h)_{\Gamma_{h,\mathrm{N}}} &\lesssim h^{q+1/2} \left[\|\boldsymbol{u}\|_{H^{\min\{q,2\}+1}(\widehat{\mathfrak{D}})} + \|\boldsymbol{g}_{\mathrm{N}}\|_{H^{\min\{q,2\}}(\widehat{\mathfrak{D}})} \right] |\!|\!| \boldsymbol{v}_h |\!|\!|_h.\end{aligned} \tag{33}$$

Proof. The first two estimates in (33) are straightforward. The last estimate uses Proposition 3. □

3.4.2 A priori estimate

Since (26) is satisfied for all $\boldsymbol{v} \in H^1(\widehat{\mathfrak{D}})$, it follows that

$$\begin{aligned} A_h(\Omega_h;\boldsymbol{u},\boldsymbol{v}_h) = \chi_h(\Omega_h;\boldsymbol{v}_h) - \big(\boldsymbol{u},\boldsymbol{\sigma}(\boldsymbol{v}_h)\boldsymbol{\nu}_h\big)_{\Gamma_{h,\mathrm{D}}} + \gamma_{\mathrm{D}}h^{-1}b(\Omega_h;\boldsymbol{u},\boldsymbol{v}_h) + \gamma_{\mathrm{N}}h\big(\boldsymbol{\sigma}(\boldsymbol{u})\boldsymbol{\nu}_h,\boldsymbol{\sigma}(\boldsymbol{v}_h)\boldsymbol{\nu}_h\big)_{\Gamma_{h,\mathrm{N}}} \\ - \gamma_{\mathrm{N}}h\big(\boldsymbol{g}_{\mathrm{N}},\boldsymbol{\sigma}(\boldsymbol{v}_h)\boldsymbol{\nu}_h\big)_{\Gamma_{h,\mathrm{N}}} + \gamma_{\mathrm{s}}s_h\Big(\mathcal{F}_{\Sigma^{\pm}_{\delta,\mathrm{D}}};\boldsymbol{u},\boldsymbol{v}_h\Big) + \gamma_{\mathrm{s}}h^2s_h\Big(\mathcal{F}_{\Sigma^{\pm}_{\delta,\mathrm{N}}};\boldsymbol{u},\boldsymbol{v}_h\Big) \quad \forall \boldsymbol{v}_h \in V_h(\Omega_h). \end{aligned} \tag{34}$$

Then, subtracting (24) we get the following pseudo Galerkin orthogonality property $\forall \boldsymbol{v}_h \in V_h(\Omega_h)$:

$$\begin{aligned} A_h(\Omega_h;\boldsymbol{u}-\boldsymbol{u}_h,\boldsymbol{v}_h) &= -\big(\boldsymbol{u},\boldsymbol{\sigma}(\boldsymbol{v}_h)\boldsymbol{\nu}_h\big)_{\Gam_{h,\mathrm{D}}} + \gamma_{\mathrm{D}}h^{-1}b(\Omega_h;\boldsymbol{u},\boldsymbol{v}_h) + \gamma_{\mathrm{N}}h\big(\boldsymbol{\sigma}(\boldsymbol{u})\boldsymbol{\nu}_h,\boldsymbol{\sigma}(\boldsymbol{v}_h)\boldsymbol{\nu}_h\big)_{\Gamma_{h,\mathrm{N}}} \\ &\quad - \gamma_{\mathrm{N}}h\big(\boldsymbol{g}_{\mathrm{N}},\boldsymbol{\sigma}(\boldsymbol{v}_h)\boldsymbol{\nu}_h\big)_{\Gamma_{h,\mathrm{N}}} + \gamma_{\mathrm{s}}s_h\Big(\mathcal{F}_{\Sigma^{\pm}_{\delta,\mathrm{D}}};\boldsymbol{u},\boldsymbol{v}_h\Big) + \gamma_{\mathrm{s}}h^2s_h\Big(\mathcal{F}_{\Sigma^{\pm}_{\delta,\mathrm{N}}};\boldsymbol{u},\boldsymbol{v}_h\Big) \\ &\lesssim \gamma_{\mathrm{s}}s_h\Big(\mathcal{F}_{\Sigma^{\pm}_{\delta,\mathrm{D}}};\boldsymbol{u},\boldsymbol{v}_h\Big) + \gamma_{\mathrm{s}}h^2s_h\Big(\mathcal{F}_{\Sigma^{\pm}_{\delta,\mathrm{N}}};\boldsymbol{u},\boldsymbol{v}_h\Big) \\ &\quad + h^q\Big[\|\boldsymbol{u}\|_{H^{\min\{q,2\}+1}(\widehat{\mathfrak{D}})} + \|\boldsymbol{g}_{\mathrm{N}}\|_{H^{\min\{q,2\}}(\widehat{\mathfrak{D}})}\Big]\|\!|\boldsymbol{v}_h|\!\|_h, \end{aligned} \tag{35}$$

where we have used (33) in the last line. From this, one can derive the following error estimate using well-known techniques.

Theorem 2. *Let $\boldsymbol{u} \in H^{k+1}(\widehat{\mathfrak{D}})$ be the extended solution of (1) on Ω to $\widehat{\mathfrak{D}}$, and let $\boldsymbol{u}_h \in V_h(\Omega_h)$ be the finite element approximation defined in (24) with $q = k \geqslant 1$. Then, the following a priori estimates hold*

$$\|\boldsymbol{u}-\boldsymbol{u}_h\|_{L^2(\Omega)} + h|\!|\!|\boldsymbol{u}-\boldsymbol{u}_h|\!|\!|_h \lesssim h^{k+1}\Big[\|\boldsymbol{u}\|_{H^{k+1}(\Omega)} + \|\boldsymbol{g}_{\mathrm{N}}\|_{H^{\min\{k,2\}}(\widehat{\mathfrak{D}})}\Big], \tag{36}$$

where standard a priori estimates give $\|\boldsymbol{u}\|_{H^{k+1}(\Omega)} \lesssim \|\boldsymbol{f}\|_{H^{k-1}(\Omega)} + \|\boldsymbol{g}_{\mathrm{N}}\|_{H^k(\Omega)}$.

4 Unfitted shape derivatives

We start with a review of basic shape differentiability results [2], [20] based on vector displacements of the domain. Next, we extend these shape derivatives to allow for perturbation of the domain by perturbing its level set description. Then, we develop these results further to allow for shape functionals over domains that intersect a fixed Lipschitz subset (i.e. an element of a finite element mesh).

4.1 Fréchet differentiability of shape functionals

We review the Fréchet Differentiability of Shape Functionals following [2], [26]. A classic approach to shape differentiation uses a perturbation of the identity. Let $\boldsymbol{U} \in [W^{1,\infty}(\mathbb{R}^d)]^d$ be a vector field and define the deformation mapping as follows

$$\boldsymbol{\Phi}_{\boldsymbol{U}}(\boldsymbol{a}) := \mathbf{id}(\boldsymbol{a}) + \boldsymbol{U}(\boldsymbol{a}) \quad \forall\, \boldsymbol{a} \in \mathbb{R}^d. \tag{37}$$

This mapping induces a deformed domain $\Omega_{\boldsymbol{U}} := \boldsymbol{\Phi}_{\boldsymbol{U}}(\Omega)$. For $\|\boldsymbol{U}\|_{W^{1,\infty}}$ sufficiently small, if Ω is Lipschitz, then $\Omega_{\boldsymbol{U}}$ will also be Lipschitz and homeomorphic to Ω [20]. We have the following definition [26, Defn. 4.1].

Definition 1. A shape functional $J(\Omega)$ is said to be *shape differentiable* at Ω if the mapping $\boldsymbol{U} \mapsto J(\Omega_{\boldsymbol{U}})$ from $[W^{1,\infty}(\mathbb{R}^d)]^d$ into $\mathbb{R}$, where $\Omega_{\boldsymbol{U}} = \boldsymbol{\Phi}_{\boldsymbol{U}}(\Omega)$ using (37), is Fréchet differentiable at $\boldsymbol{U} = \mathbf{0}$. The Fréchet derivative of J at Ω is an operator in $\mathcal{L}([W^{1,\infty}(\mathbb{R}^d)]^d, \mathbb{R})$, denoted $J'(\Omega)(\cdot)$, and the following limit holds

$$\lim_{\|\boldsymbol{U}\|_{W^{1,\infty}}\to 0} \frac{|J(\Omega_{\boldsymbol{U}}) - J(\Omega) - J'(\Omega)(\boldsymbol{U})|}{\|\boldsymbol{U}\|_{W^{1,\infty}}} = 0. \tag{38}$$

We note a classic expansion of the determinant that is easily derived from [6, Lem. B.2].

Lemma 1. *For any $n \times n$ matrix B, we have*

$$\det(I+B) = 1 + \operatorname{tr}(B) + \frac{1}{2}\left[(\operatorname{tr}(B))^2 - \operatorname{tr}\left(B^2\right)\right] + o(|B|^2) \quad \text{as } |B| \to 0. \tag{39}$$

The next two lemmas are applications of results in refs. [2], [20]. We include the proof of Lemma 3 since we build on it later when computing shape derivatives on "cut" elements.

Lemma 2. *Given $f \in L^1(\mathbb{R}^d)$ and $\boldsymbol{U} \in [W^{1,\infty}(\mathbb{R}^d)]^d$ we have that*

$$\lim_{\|\boldsymbol{U}\|_{W^{1,\infty}} \to 0} \frac{\int_\Omega \left[f(\boldsymbol{\Phi}_{\boldsymbol{U}}(\boldsymbol{a})) - f(\boldsymbol{a})\right] G(\nabla_{\boldsymbol{a}} \boldsymbol{U}(\boldsymbol{a}))\mathrm{d}\boldsymbol{a}}{\|\boldsymbol{U}\|_{W^{1,\infty}}} = 0, \tag{40}$$

where $G\colon \mathbb{R}^{d\times d} \to \mathbb{R}$ is continuous and $|G(M)| \leqslant C|M|$ for all $M \in \mathbb{R}^{d\times d}$, for some bounded constant $C > 0$.

Lemma 3. *Given $f \in W^{1,1}(\mathbb{R}^d)$ and $\boldsymbol{U} \in [W^{1,\infty}(\mathbb{R}^d)]^d$ we have that*

$$\lim_{\|\boldsymbol{U}\|_{W^{1,\infty}} \to 0} \frac{\int_\Omega f(\boldsymbol{\Phi}_{\boldsymbol{U}}(\boldsymbol{a})) - f(\boldsymbol{a})\mathrm{d}\boldsymbol{a} - \int_\Omega \nabla f(\boldsymbol{a}) \cdot \boldsymbol{U}(\boldsymbol{a})\mathrm{d}\boldsymbol{a}}{\|\boldsymbol{U}\|_{W^{1,\infty}}} = 0. \tag{41}$$

Proof. By the fundamental theorem of calculus, we have

$$I_0(\boldsymbol{U}) := \int_\Omega f(\boldsymbol{\Phi}_{\boldsymbol{U}}(\boldsymbol{a})) - f(\boldsymbol{a})\mathrm{d}\boldsymbol{a} - \int_\Omega \nabla f(\boldsymbol{a}) \cdot \boldsymbol{U}(\boldsymbol{a})\mathrm{d}\boldsymbol{a} = \int_\Omega \int_0^1 \left[\nabla f(\boldsymbol{\Phi}_{s\boldsymbol{U}}(\boldsymbol{a})) - \nabla f(\boldsymbol{a})\right] \cdot \boldsymbol{U}(\boldsymbol{a})\mathrm{d}s\mathrm{d}\boldsymbol{a}, \tag{42}$$

and note that by Proposition 2, $\nabla f \circ \boldsymbol{\Phi}_{s\boldsymbol{U}}(\boldsymbol{a})$ can be viewed as function in $L^1(\mathbb{R}^d \times [0,1])$, provided $\|\boldsymbol{U}\|_{W^{1,\infty}}$ is sufficiently small. Indeed, the entire integrand in the last integral of (42) is in $L^1(\mathbb{R}^d \times [0,1])$.

Therefore, we can apply Fubini's theorem:

$$\begin{aligned}\frac{|I_0(\boldsymbol{U})|}{\|\boldsymbol{U}\|_{W^{1,\infty}}} &= \frac{1}{\|\boldsymbol{U}\|_{W^{1,\infty}}} \left| \int_0^1 \int_\Omega \left[\nabla f(\boldsymbol{\Phi}_{s\boldsymbol{U}}(\boldsymbol{a})) - \nabla f(\boldsymbol{a})\right] \cdot \boldsymbol{U}(\boldsymbol{a})\mathrm{d}\boldsymbol{a}\mathrm{d}s \right| \leqslant \int_0^1 \int_\Omega \left|\nabla f(\boldsymbol{\Phi}_{s\boldsymbol{U}}(\boldsymbol{a})) - \nabla f(\boldsymbol{a})\right| \mathrm{d}\boldsymbol{a}\mathrm{d}s \\ &\leqslant \int_0^1 \int_\Omega \left|\nabla(f - f_k)(\boldsymbol{\Phi}_{s\boldsymbol{U}}(\boldsymbol{a}))\right| \mathrm{d}\boldsymbol{a}\mathrm{d}s + \int_0^1 \int_\Omega \left|\nabla(f - f_k)(\boldsymbol{a})\right| \mathrm{d}\boldsymbol{a}\mathrm{d}s + \int_0^1 \int_\Omega \left|\nabla f_k(\boldsymbol{\Phi}_{s\boldsymbol{U}}(\boldsymbol{a})) - \nabla f_k(\boldsymbol{a})\right| \mathrm{d}\boldsymbol{a}\mathrm{d}s,\end{aligned} \tag{43}$$

where we introduced the sequence $\{f_k\}$ in $C^\infty(\mathbb{R}^d)$ such that $f_k \to f$ in $W^{1,1}$ as $k \to \infty$. We apply a change of variables to the first term:

$$\int_0^1 \int_\Omega \left|\nabla(f - f_k)(\boldsymbol{\Phi}_{s\boldsymbol{U}}(\boldsymbol{a}))\right| \mathrm{d}\boldsymbol{a}\mathrm{d}s = \int_0^1 \int_{\boldsymbol{\Phi}_{s\boldsymbol{U}}^{-1}(\Omega)} \left|\nabla(f - f_k)(\boldsymbol{x})\right| \det(\nabla \boldsymbol{\Phi}_{s\boldsymbol{U}}^{-1}(\boldsymbol{x}))\mathrm{d}\boldsymbol{x}\mathrm{d}s \leqslant \gamma_0 \|f - f_k\|_{W^{1,1}(\mathbb{R}^d)}, \tag{44}$$

where γ_0 is a bounded constant when $\|\boldsymbol{U}\|_{W^{1,\infty}(\mathbb{R}^d)}$ is sufficiently small. The last term in (43) is estimated with the mean value theorem to give

$$\int_0^1 \int_\Omega \left|\nabla f_k(\boldsymbol{\Phi}_{s\boldsymbol{U}}(\boldsymbol{a})) - \nabla f_k(\boldsymbol{a})\right| \mathrm{d}\boldsymbol{a}\mathrm{d}s \leqslant C_k \|\boldsymbol{U}\|_{L^\infty(\mathbb{R}^d)}, \tag{45}$$

where C_k depends on $\|\nabla\nabla f_k\|_{L^\infty}$. Thus,

$$\lim_{\|\boldsymbol{U}\|_{W^{1,\infty}}\to 0} \frac{|I_0(\boldsymbol{U})|}{\|\boldsymbol{U}\|_{W^{1,\infty}}} \leqslant (\gamma_0+1)\|f-f_k\|_{W^{1,1}(\mathbb{R}^d)}, \tag{46}$$

which holds for every $k \geqslant 1$. Taking $k\to\infty$ proves (41). □

The following result is an application of the results in refs. [2], [20], [26].

Theorem 3. *For the shape functional $J(\Omega) := \int_\Omega f(\boldsymbol{x})\mathrm{d}\boldsymbol{x}$, with $f \in W^{1,1}(\mathbb{R}^d)$ and Ω Lipschitz, we have that $J(\Omega)$ is shape differentiable at Ω (in the sense of Definition 1) with Fréchet derivative $J'(\Omega)(\boldsymbol{U}) = \int_{\partial\Omega} f(\boldsymbol{a})\boldsymbol{U}(\boldsymbol{a})\cdot\boldsymbol{\nu}(\boldsymbol{a})\mathrm{d}\boldsymbol{a}$ for all $\boldsymbol{U}\in[W^{1,\infty}(\mathbb{R}^d)]^d$.*

4.2 Connecting the domain perturbation with the level set perturbation

Our goal is to obtain a shape differentiation formula in terms of perturbations of the level set representation ϕ of Ω (see Section 3.1), since this is more convenient for the optimization algorithm. Direct optimization of the level set function was also considered in ref. [49], which used finite differences and was an example of the optimize-then-discretize approach. In ref. [50], they developed Gâteaux derivative formulas for direct perturbation of smooth level set functions; similar considerations were also made in ref. [20].

4.2.1 The speed method

We review the velocity (speed) method for domain perturbations. Let $\boldsymbol{V}(\boldsymbol{x},t)$ be a d-dimensional, vector field that is Lipschitz in $\boldsymbol{x}$, for each t, and continuously differentiable in t for each $\boldsymbol{x}$. For any given $\boldsymbol{a}\in\mathbb{R}^d$, consider the following ODE:

$$\dot{\boldsymbol{x}} = \boldsymbol{V}(\boldsymbol{x},t) \quad \forall\, t>0, \qquad \boldsymbol{x}(0)=\boldsymbol{a}\in\mathbb{R}^d, \tag{47}$$

with unique solution (see [51]) $\boldsymbol{x}(t)$ being the trajectory of a (material) point $\boldsymbol{a}$ moving with velocity $\boldsymbol{V}(\boldsymbol{x}(t),t)$. Indeed, $\boldsymbol{V}$ induces a deformation mapping through (47) in the following way. Let $\boldsymbol{x}(t;\ \boldsymbol{a})$ be the unique solution of (47) (for a given $\boldsymbol{a}$). Then,

$$\boldsymbol{\Phi}_t(\boldsymbol{a}) := \boldsymbol{x}(t;\boldsymbol{a}) \quad \forall\ \boldsymbol{a}\in\mathbb{R}^d, \tag{48}$$

is the corresponding deformation mapping. Moreover, a Taylor expansion in t yields

$$\boldsymbol{\Phi}_t(\boldsymbol{a}) = \boldsymbol{a} + t\boldsymbol{V}(\boldsymbol{a},0) + \boldsymbol{W}(\boldsymbol{a},t) \quad \forall\ \boldsymbol{a}\in\mathbb{R}^d, \tag{49}$$

where $|\boldsymbol{W}(\boldsymbol{a},t)| = O(t^2)$. With this, one can establish the Gâteaux shape differentiablity of our shape functional $J(\Omega) = \int_\Omega f(\boldsymbol{x})\,\mathrm{d}\boldsymbol{x}$, for $f\in W^{1,1}(\mathbb{R}^d)$, with respect to $\boldsymbol{V}(\boldsymbol{x}(0),0)$ using classic techniques. In other words, setting $\Omega_t = \boldsymbol{\Phi}_t(\Omega)$, we have

$$d_G J(\Omega)(\boldsymbol{V}) := \lim_{t\to 0^+}\frac{J(\Omega_t)-J(\Omega)}{t} = \int_{\partial\Omega} f(\boldsymbol{a})\boldsymbol{V}(\boldsymbol{a},0)\cdot\boldsymbol{\nu}(\boldsymbol{a})\mathrm{d}\boldsymbol{a}, \tag{50}$$

which, of course, agrees with the result in Theorem 3 if $\boldsymbol{U}(\boldsymbol{a})\equiv\boldsymbol{V}(\boldsymbol{a},0)$. The same result holds if the remainder term in (49) is dropped.

4.2.2 Level set Gâteaux derivative

Now, we consider Ω to be defined by a level set function, ϕ, i.e. $\Omega(\phi) := \{\boldsymbol{x}\in\mathbb{R}^d \mid \phi(\boldsymbol{x})<0\}$ (sub-zero level set), where ϕ satisfies Definition 2 for some positive constants c_0 and δ_0.

Definition 2. Let $\phi\in C^{0,1}(\mathbb{R}^d;\mathbb{R})$ and assume that $\Gamma(\phi) := \{\boldsymbol{x}\in\mathbb{R}^d \mid \phi(\boldsymbol{x})=0\}$ is non-empty. We say that ϕ is *non-degenerate, with constants $c_0>0$ and $\delta_0>0$*, if $|\nabla\phi(\boldsymbol{x})|\geqslant c_0$ for a.e. $\boldsymbol{x}\in\mathbb{R}^d$ such that $\mathrm{dist}(\boldsymbol{x},\Gamma(\phi))<\delta_0$.

In addition, we take ϕ to be $C^2(\mathbb{R}^d)$. By [20, Ch. 2, Thm. 4.2], $\Omega(\phi)$ is a C^2, open set, and $\partial\Omega(\phi) \equiv \Gamma(\phi)$, so $\Omega(\phi)$ is well-defined.

For the shape functional, $J(\Omega)$, we seek to compute the Gâteaux shape derivative with respect to ϕ, i.e.

$$d_G J(\Omega(\phi))(\eta) := \lim_{t\to 0^+} \frac{J(\Omega(\phi + t\eta)) - J(\Omega(\phi))}{t} \tag{51}$$

for any $\eta \in C^2(\mathbb{R}^d)$. Define a perturbed level set function

$$\tilde{\phi}(\boldsymbol{x}, t) = \phi(\boldsymbol{x}) + t\eta(\boldsymbol{x}) \quad \Rightarrow \quad \partial_t \tilde{\phi} = \eta, \tag{52}$$

where t is the perturbation parameter; one can think of $\tilde{\phi}$ as a time-dependent level set function. Set $\Omega_t := \Omega(\tilde{\phi}(\cdot, t)) = \{\boldsymbol{x} \in \mathbb{R}^d \mid \tilde{\phi}(\boldsymbol{x}, t) < 0\}$ and $\Gamma_t := \partial\Omega_t = \{\boldsymbol{x} \in \mathbb{R}^d \mid \tilde{\phi}(\boldsymbol{x}, t) = 0\}$. Note that $|\nabla\tilde{\phi}(\boldsymbol{x}, t)| \geqslant c_0/2 > 0$ for all $\boldsymbol{x}$ in a neighborhood of Γ_t if t is sufficiently small. This ensures that Γ_t is (locally) a C^2 surface by the implicit function theorem. Next, define a velocity field

$$\boldsymbol{V}(\boldsymbol{x}, t) = -\frac{\nabla\tilde{\phi}(\boldsymbol{x}, t)}{|\nabla\tilde{\phi}(\boldsymbol{x}, t)|^2}\eta(\boldsymbol{x}), \tag{53}$$

which satisfies the same conditions for $\boldsymbol{V}$ in (47), and let $\boldsymbol{x}(t)$ be the corresponding solution of (47). If $\boldsymbol{a} \in \Gamma_0$, we have that $\tilde{\phi}(\boldsymbol{x}(t), t) = 0$ for all t because

$$\begin{aligned} \frac{\mathrm{d}}{\mathrm{d}t}\tilde{\phi}(\boldsymbol{x}(t), t) \equiv D_{\boldsymbol{V}}\tilde{\phi}(\boldsymbol{x}, t)\Big|_{\boldsymbol{x}=\boldsymbol{x}(t)} &= \partial_t\tilde{\phi}(\boldsymbol{x}, t)\Big|_{\boldsymbol{x}=\boldsymbol{x}(t)} + \left(\nabla\tilde{\phi}(\boldsymbol{x}, t)\Big|_{\boldsymbol{x}=\boldsymbol{x}(t)}\right) \cdot \dot{\boldsymbol{x}}(t) \\ &= \eta(\boldsymbol{x}(t)) + \nabla\tilde{\phi}(\boldsymbol{x}(t), t) \cdot \boldsymbol{V}(\boldsymbol{x}(t), t) = 0, \end{aligned} \tag{54}$$

and the fact that $\tilde{\phi}(\boldsymbol{x}(0), 0) = 0$. Thus, $\boldsymbol{V}$ evolves the zero level set of $\tilde{\phi}$. Moreover, if $\boldsymbol{\Phi}_t(\boldsymbol{a})$ is the induced map from $\boldsymbol{V}$, then the sub-zero level set Ω_t satisfies $\Omega_t = \boldsymbol{\Phi}_t(\Omega_0)$.

With this, one can compute (51) by using (50), i.e.

$$\begin{aligned} d_G J(\Omega(\phi))(\eta) = \lim_{t\to 0^+} \frac{J(\Omega(\phi + t\eta)) - J(\Omega(\phi))}{t} &= \lim_{t\to 0^+} \frac{J(\Omega_t) - J(\Omega_0)}{t} = \int_{\partial\Omega} f(\boldsymbol{a})\boldsymbol{V}(\boldsymbol{a}, 0) \cdot \boldsymbol{\nu}(\boldsymbol{a})\mathrm{d}\boldsymbol{a} \\ = \int_{\partial\Omega} f(\boldsymbol{a})\left(-\frac{\nabla\tilde{\phi}(\boldsymbol{a}, 0)}{|\nabla\tilde{\phi}(\boldsymbol{a}, 0)|^2}\eta(\boldsymbol{a})\right) \cdot \boldsymbol{\nu}(\boldsymbol{a})\mathrm{d}\boldsymbol{a} &= \int_{\partial\Omega} f(\boldsymbol{a})\left(-\frac{\eta(\boldsymbol{a})}{|\nabla\phi(\boldsymbol{a})|}\right)\mathrm{d}\boldsymbol{a}, \end{aligned} \tag{55}$$

where we used the fact that $\boldsymbol{\nu} = \nabla\phi/|\nabla\phi|$ on $\partial\Omega$ and $\tilde{\phi}(\boldsymbol{a}, 0) = \phi(\boldsymbol{a})$. All of the above extends to having ϕ, η in $W^{2,\infty}(\mathbb{R}^d)$; in this case, $\Omega(\phi)$ is a $C^{1,1}$ domain [20, Ch. 5, Thm 4.3].

4.2.3 Level set Fréchet derivative

Our goal now is to extend this to computing the Fréchet shape derivative of $J(\Omega(\phi))$ with respect to ϕ, which is defined as follows.

Definition 3. Let $\Omega = \Omega(\phi)$ be the sub-zero level set of $\phi \in \mathcal{X}$, such that $|\nabla\phi| \geqslant c_0 > 0$, for some positive constant c_0. A shape functional $J(\phi) \equiv J(\Omega(\phi))$ is said to be *level set shape Fréchet differentiable* at ϕ if the mapping $\eta \mapsto J(\Omega(\phi + \eta))$ from $\mathcal{X}$ into $\mathbb{R}$ is Fréchet differentiable at $\eta = 0$. The Fréchet derivative of $J(\Omega(\cdot))$, at ϕ, is an operator in $\mathcal{L}(\mathcal{X}, \mathbb{R})$, denoted $J'(\Omega(\phi))(\cdot)$, and the following limit holds

$$\lim_{\|\eta\|_{\mathcal{X}}\to 0} \frac{|J(\Omega(\phi + \eta)) - J(\Omega(\phi)) - J'(\Omega(\phi))(\eta)|}{\|\eta\|_{\mathcal{X}}} = 0. \tag{56}$$

In this section, we use Definition 3 with $\mathcal{X} = W^{2,\infty}(\mathbb{R}^d)$. Moreover, we shall prove that $J(\Omega) = \int_\Omega f(\boldsymbol{x})\,\mathrm{d}\boldsymbol{x}$ is level set shape Fréchet differentiable by using Theorem 3. To do this, we have to reconcile two different, but

similar, notions of domain perturbation. The first is the perturbed domain $\Omega(\phi + \eta)$ and the second is through a perturbation of the identity approach given by

$$\boldsymbol{\Phi}_\eta(\boldsymbol{a}) = \boldsymbol{a} + \boldsymbol{V}_\eta(\boldsymbol{a}) \quad \forall\, \boldsymbol{a} \in \mathbb{R}^d, \quad \boldsymbol{V}_\eta(\boldsymbol{a}) := -\frac{\nabla\phi(\boldsymbol{a})}{|\nabla\phi(\boldsymbol{a})|^2}\eta(\boldsymbol{a}). \tag{57}$$

Note the similarity with (49) and (53). Let $\boldsymbol{\Phi}_t$ (different from $\boldsymbol{\Phi}_\eta$) satisfy (47) with $\boldsymbol{V}$ given by (53), and note that $\nabla_{\boldsymbol{a}}\boldsymbol{\Phi}_t(\boldsymbol{a})$ uniquely satisfies the matrix valued ODE [20, Ch. 8]:

$$\frac{\mathrm{d}}{\mathrm{d}t}M(\boldsymbol{a},t) = [\nabla_{\boldsymbol{x}}\boldsymbol{V}(\boldsymbol{\Phi}_t(\boldsymbol{a}),t)]M(\boldsymbol{a},t) \quad \forall\, t>0, \quad M(\boldsymbol{a},0) = I \quad \forall\, \boldsymbol{a}\in\mathbb{R}^d, \tag{58}$$

which follows by the theory in ref. [51]. Furthermore, we have an explicit formula for $\nabla_{\boldsymbol{a}}\boldsymbol{\Phi}_t(\boldsymbol{a})$:

$$\nabla_{\boldsymbol{a}}\boldsymbol{\Phi}_t(\boldsymbol{a}) = \exp\left\{\int_0^t \nabla_{\boldsymbol{x}}\boldsymbol{V}(\boldsymbol{x}(s;\boldsymbol{a}),s)\,\mathrm{d}s\right\} =: A(t), \tag{59}$$

where $\exp\{\cdot\}$ is the matrix exponential.

Theorem 4. *Let $\{\phi_k\}_{k\geqslant 1}$ be a sequence of smooth functions such that $\|\phi_k - \phi\|_{W^{2,\infty}} \to 0$ as $k\to\infty$. Assume $|\nabla\phi| \geqslant c_0 > 0$ and $|\nabla\eta| \leqslant c_0/2$, so that $|\nabla(\phi+\eta)| \geqslant c_0/2$. In addition, assume $\|\eta\|_{W^{2,\infty}} \leqslant c_1$ for some fixed constant c_1. Set $\widetilde{\boldsymbol{\Phi}} = \boldsymbol{\Phi}_t|_{t=1}$. Then,*

$$\begin{aligned}
\|\boldsymbol{\Phi}_\eta - \widetilde{\boldsymbol{\Phi}}\|_{L^\infty(\mathbb{R}^d)} &\leqslant O\big(\|\eta\|_{L^\infty}\|\nabla\eta\|_{L^\infty}\big),\\
\|\nabla\boldsymbol{\Phi}_\eta - \nabla\widetilde{\boldsymbol{\Phi}}\|_{L^\infty(\mathbb{R}^d)} &\leqslant O\Big(\|\eta\|^2_{W^{2,\infty}}\Big) + q_1\|\phi_k\|_{W^{3,\infty}}\|\eta\|^2_{L^\infty} + q_2\|\phi_k-\phi\|_{W^{2,\infty}}\|\eta\|_{L^\infty}
\end{aligned} \tag{60}$$

for all $k \geqslant 1$, for some bounded constants q_1, q_2.

Proof. Recall that $\boldsymbol{\Phi}_t$ is defined in Section 4.2.1 and is different from $\boldsymbol{\Phi}_\eta$. For now, take $\boldsymbol{a}\in\mathbb{R}^d$ fixed and note that the solution of (47) satisfies:

$$|\boldsymbol{x}(t) - \boldsymbol{a}| = \left|\int_0^t \boldsymbol{V}(\boldsymbol{x}(s),s)\,\mathrm{d}s\right| \leqslant C\big(\|\phi\|_{W^{1,\infty}} + \|\eta\|_{W^{1,\infty}}\big)\|\eta\|_{L^\infty},\ 0\leqslant t\leqslant 1, \tag{61}$$

for some constant C depending on c_0. We first estimate $\|\boldsymbol{\Phi}_\eta - \widetilde{\boldsymbol{\Phi}}\|_{L^\infty(\mathbb{R}^d)}$ and we start with

$$\begin{aligned}
\boldsymbol{V}_\eta(\boldsymbol{a}) - \boldsymbol{V}(\boldsymbol{x}(s),s) &= -\left[\frac{\nabla\phi(\boldsymbol{a})}{|\nabla\phi(\boldsymbol{a})|^2}\eta(\boldsymbol{a}) - \frac{\nabla[\phi(\boldsymbol{x}(s)) + s\eta(\boldsymbol{x}(s))]}{|\nabla[\phi(\boldsymbol{x}(s)) + s\eta(\boldsymbol{x}(s))]|^2}\eta(\boldsymbol{x}(s))\right]\\
&= T_1 + T_2 + T_3,
\end{aligned} \tag{62}$$

where

$$\begin{aligned}
T_1 &= \frac{1}{|\nabla\phi(\boldsymbol{a})|^2}\big(\eta(\boldsymbol{a})\nabla\phi(\boldsymbol{a}) - \eta(\boldsymbol{x}(s))\nabla\phi(\boldsymbol{x}(s))\big),\\
T_2 &= -\frac{s}{|\nabla\phi(\boldsymbol{a})|^2}\eta(\boldsymbol{x}(s))\nabla\eta(\boldsymbol{x}(s)),\\
T_3 &= \eta(\boldsymbol{x}(s))\nabla[\phi(\boldsymbol{x}(s)) + s\eta(\boldsymbol{x}(s))]\left(\frac{|\nabla[\phi(\boldsymbol{x}(s)) + s\eta(\boldsymbol{x}(s))]|^2 - |\nabla\phi(\boldsymbol{a})|^2}{|\nabla\phi(\boldsymbol{a})|^2|\nabla[\phi(\boldsymbol{x}(s)) + s\eta(\boldsymbol{x}(s))]|^2}\right).
\end{aligned} \tag{63}$$

Next, we note the following basic estimates:

$$\begin{aligned}
|\nabla\phi(\boldsymbol{x}(s)) - \nabla\phi(\boldsymbol{a})| = |\nabla^2\phi(\boldsymbol{x}(\xi))\cdot(\boldsymbol{x}(s)-\boldsymbol{a})| &\leqslant C\|\nabla^2\phi\|_{L^\infty}\|\eta\|_{L^\infty},\\
|\eta(\boldsymbol{x}(s)) - \eta(\boldsymbol{a})| &\leqslant C\|\nabla\eta\|_{L^\infty}\|\eta\|_{L^\infty}
\end{aligned} \tag{64}$$

for some bounded constant C. Using these estimates, it is easy to show that

$$|T_1|, |T_2|, |T_3| \leqslant C\|\eta\|_{L^\infty}\|\nabla\eta\|_{L^\infty} \tag{65}$$

for some bounded constant C, which gives a bound for (62). Since $\boldsymbol{x}(1) \equiv \tilde{\boldsymbol{\Phi}}(\boldsymbol{a}) = \boldsymbol{a} + \int_0^1 \boldsymbol{V}(\boldsymbol{x}(s), s)\mathrm{d}s$, and $\boldsymbol{a}$ was arbitrary, we get

$$\|\boldsymbol{\Phi}_\eta - \tilde{\boldsymbol{\Phi}}\|_{L^\infty(\mathbb{R}^d)} = \left\| \int_0^1 \boldsymbol{V}_\eta(\boldsymbol{a}) - \boldsymbol{V}(\boldsymbol{x}(s), s)\ \mathrm{d}s \right\| \leqslant C\|\eta\|_{L^\infty}\|\nabla\eta\|_{L^\infty}. \tag{66}$$

Next, using that $\boldsymbol{V}_\eta(\boldsymbol{a}) \equiv \boldsymbol{V}(\boldsymbol{a}, 0)$, we estimate

$$\begin{aligned} \nabla\boldsymbol{V}(\boldsymbol{x}(s), s)A(s) - \nabla\boldsymbol{V}(\boldsymbol{a}, 0) &= T_4 + T_5, \\ T_4 &:= \big[\nabla\boldsymbol{V}(\boldsymbol{x}(s), s) - \nabla\boldsymbol{V}_\eta(\boldsymbol{a})\big]A(s), \\ T_5 &:= \nabla\boldsymbol{V}_\eta(\boldsymbol{a})\big[A(s) - I\big]. \end{aligned} \tag{67}$$

Estimating T_4 is similar to estimating (63). We first note that $|\nabla\eta(\boldsymbol{x}(s)) - \nabla\eta(\boldsymbol{a})| \leqslant C\|\nabla^2\eta\|_{L^\infty}\|\eta\|_{L^\infty}$, for some bounded constant C. Furthermore,

$$\begin{aligned} |\nabla^2\phi(\boldsymbol{x}(s)) - \nabla^2\phi(\boldsymbol{a})| &\leqslant |\nabla^2(\phi - \phi_k)(\boldsymbol{x}(s)) - \nabla^2(\phi - \phi_k)(\boldsymbol{a})| + |\nabla^2\phi_k(\boldsymbol{x}(s)) - \nabla^2\phi_k(\boldsymbol{a})| \\ &\leqslant 2\|\phi - \phi_k\|_{W^{2,\infty}} + |\nabla^3\phi_k(\boldsymbol{x}(\xi)) \cdot (\boldsymbol{x}(s) - \boldsymbol{a})| \\ &\leqslant 2\|\phi - \phi_k\|_{W^{2,\infty}} + C\|\nabla^3\phi_k\|_{L^\infty}\|\eta\|_{L^\infty} \end{aligned} \tag{68}$$

for every $k \geqslant 1$. Next, by the properties of the matrix exponential, we have

$$|A(s) - I| \leqslant \int_0^s \left|\nabla_{\boldsymbol{x}}\boldsymbol{V}(\boldsymbol{x}(\mu; \boldsymbol{a}), \mu)\right| \mathrm{d}\mu |A|(s), \quad |A|(s) = \exp\left\{ \int_0^s \left|\nabla_{\boldsymbol{x}}\boldsymbol{V}(\boldsymbol{x}(\mu; \boldsymbol{a}), \mu)\right| \mathrm{d}\mu \right\}. \tag{69}$$

Note that $|A(s)|$ is uniformly bounded for all $0 \leqslant s \leqslant 1$, and $\left|\nabla_{\boldsymbol{x}}\boldsymbol{V}(\boldsymbol{x}(\mu; \boldsymbol{a}), \mu)\right| \leqslant C\|\eta\|_{W^{1,\infty}}$. Combining these estimates, and the usual arguments, we have

$$|\nabla\boldsymbol{V}(\boldsymbol{x}(s), s)A(s) - \nabla\boldsymbol{V}(\boldsymbol{a}, 0)| \leqslant C\Big(\|\eta\|_{W^{2,\infty}}^2 + \|\phi - \phi_k\|_{W^{2,\infty}}\|\eta\|_{L^\infty} + \|\nabla^3\phi_k\|_{L^\infty}\|\eta\|_{L^\infty}^2 \Big) \tag{70}$$

for all $0 \leqslant s \leqslant 1$. From this, we obtain the bound on $\|\nabla\boldsymbol{\Phi}_\eta - \nabla\widetilde{\boldsymbol{\Phi}}\|_{L^\infty}$ given in (60). □

Corollary 2. *Assume the hypothesis of Theorem 4 holds. Then,*

$$\|\det(\nabla\boldsymbol{\Phi}_\eta) - \det(\nabla\widetilde{\boldsymbol{\Phi}})\|_{L^\infty(\mathbb{R}^d)} \leqslant O\Big(\|\eta\|_{W^{2,\infty}}^2 \Big) + q_1\|\phi_k\|_{W^{3,\infty}}\|\eta\|_{L^\infty}^2 + q_2\|\phi_k - \phi\|_{W^{2,\infty}}\|\eta\|_{L^\infty} \tag{71}$$

for all $k \geqslant 1$, for some bounded constants q_1, q_2.

Theorem 5. *Assume $\phi \in W^{2,\infty}(\mathbb{R}^d)$ and that it satisfies Definition 2 for some positive constants c_0, δ_0. Let $\Omega(\phi + \eta)$ be the sub-zero level set of $\phi + \eta$. For the shape functional $J(\Omega) := \int_\Omega f(\boldsymbol{x})\mathrm{d}\boldsymbol{x}$ with $f \in W^{1,1}(\mathbb{R}^d)$ we have that $J(\Omega)$ is level set shape differentiable at Ω (in the sense of Definition 3 with $\mathcal{X} = W^{2,\infty}(\mathbb{R}^d)$) with Fréchet derivative $J'(\Omega)(\eta) = \int_{\partial\Omega} f(\boldsymbol{a})\big(-\eta(\boldsymbol{a})|\nabla\phi(\boldsymbol{a})|^{-1}\big)\mathrm{d}\boldsymbol{a}$ for all $\eta \in W^{2,\infty}(\mathbb{R}^d)$.*

Proof. First note that $\Omega(\phi + \eta) = \Omega_1 = \boldsymbol{\Phi}_1(\Omega_0) \equiv \widetilde{\boldsymbol{\Phi}}(\Omega)$ and $\Omega(\phi) = \Omega_0 \equiv \Omega$. In addition,

$$J'(\Omega(\phi))(\eta) = \int_{\partial\Omega(\phi)} f(\boldsymbol{a})\left(-\frac{\eta(\boldsymbol{a})}{|\nabla\phi(\boldsymbol{a})|} \right)\mathrm{d}\boldsymbol{a} = \int_{\partial\Omega} f(\boldsymbol{a})\boldsymbol{V}_\eta(\boldsymbol{a}) \cdot \boldsymbol{\nu}\ \mathrm{d}\boldsymbol{a} = J'(\Omega)(\boldsymbol{V}_\eta),$$

where $\boldsymbol{V}_\eta$ is given by (57). Now, note that

$$\begin{aligned} J(\Omega(\phi+\eta)) &= \int_{\widetilde{\boldsymbol{\Phi}}(\Omega)} f(\boldsymbol{x})\mathrm{d}\boldsymbol{x} - \int_{\boldsymbol{\Phi}_\eta(\Omega)} f(\boldsymbol{x})\mathrm{d}\boldsymbol{x} + \underbrace{\int_{\boldsymbol{\Phi}_\eta(\Omega)} f(\boldsymbol{x})\mathrm{d}\boldsymbol{x}}_{=J(\Omega_{\boldsymbol{V}_\eta})} \\ &= \underbrace{\int_\Omega f(\widetilde{\boldsymbol{\Phi}}(\boldsymbol{a}))\det(\nabla_{\boldsymbol{a}}\widetilde{\boldsymbol{\Phi}}(\boldsymbol{a}))\mathrm{d}\boldsymbol{a} - \int_\Omega f(\boldsymbol{\Phi}_\eta(\boldsymbol{a}))\det(\nabla_{\boldsymbol{a}}\boldsymbol{\Phi}_\eta(\boldsymbol{a}))\mathrm{d}\boldsymbol{a}}_{=T_6} + J(\Omega_{\boldsymbol{V}_\eta}). \end{aligned} \tag{72}$$

By the fundamental theorem of calculus, we have

$$f(\widetilde{\boldsymbol{\Phi}}(\boldsymbol{a})) - f(\boldsymbol{\Phi}_\eta(\boldsymbol{a})) = \int_0^1 \nabla f\Big(s\widetilde{\boldsymbol{\Phi}}(\boldsymbol{a}) + (1-s)\boldsymbol{\Phi}_\eta(\boldsymbol{a})\Big)\cdot\Big(\widetilde{\boldsymbol{\Phi}}(\boldsymbol{a}) - \boldsymbol{\Phi}_\eta(\boldsymbol{a})\Big)\mathrm{d}s, \tag{73}$$

and so

$$\begin{aligned} |T_6| &\leqslant \int_\Omega \Big(f(\widetilde{\boldsymbol{\Phi}}(\boldsymbol{a})) - f(\boldsymbol{\Phi}_\eta(\boldsymbol{a}))\Big)\det(\nabla_{\boldsymbol{a}}\widetilde{\boldsymbol{\Phi}}(\boldsymbol{a}))\mathrm{d}\boldsymbol{a} + \int_\Omega f(\boldsymbol{\Phi}_\eta(\boldsymbol{a}))\Big(\det(\nabla_{\boldsymbol{a}}\widetilde{\boldsymbol{\Phi}}(\boldsymbol{a})) - \det(\nabla_{\boldsymbol{a}}\boldsymbol{\Phi}_\eta(\boldsymbol{a}))\Big)\mathrm{d}\boldsymbol{a} \\ &\leqslant C\|f\|_{W^{1,1}(\mathbb{R}^d)}\|\nabla\eta\|_{L^\infty}^2 + C\|f\|_{L^1(\mathbb{R}^d)}\Big(\|\eta\|_{W^{2,\infty}}^2 + \|\phi_k\|_{W^{3,\infty}}\|\eta\|_{L^\infty}^2 + \|\phi_k-\phi\|_{W^{2,\infty}}\|\eta\|_{L^\infty}\Big), \end{aligned} \tag{74}$$

where we used Theorem 4 and Corollary 2. Therefore,

$$J(\Omega(\phi+\eta)) - J(\Omega(\phi)) - J'(\Omega(\phi))(\eta) = T_6 + J(\Omega_{\boldsymbol{V}_\eta}) - J(\Omega) - J'(\Omega)(\boldsymbol{V}_\eta), \tag{75}$$

and since $\|\boldsymbol{V}_\eta\|_{W^{1,\infty}} \leqslant C_\eta\|\eta\|_{W^{1,\infty}}$, for all $k \geqslant 1$, we obtain

$$\begin{aligned} &\lim_{\|\eta\|_{W^{2,\infty}}\to 0} \frac{|J(\Omega(\phi+\eta)) - J(\Omega(\phi)) - J'(\Omega(\phi))(\eta)|}{\|\eta\|_{W^{2,\infty}}} \\ &\qquad \leqslant C\|\phi_k-\phi\|_{W^{2,\infty}} + C_\eta \lim_{\|\boldsymbol{V}_\eta\|_{W^{1,\infty}}\to 0} \frac{|J(\Omega_{\boldsymbol{V}_\eta}) - J(\Omega) - J'(\Omega)(\boldsymbol{V}_\eta)|}{\|\boldsymbol{V}_\eta\|_{W^{1,\infty}}} \leqslant C\|\phi_k-\phi\|_{W^{2,\infty}}, \end{aligned} \tag{76}$$

where we used Theorem 3. Taking $k\to\infty$ proves the result. □

4.3 Shape differentiability on a cut subdomain

We now extend the above formula to computing shape derivatives when Ω is "cut" by another fixed domain. In other words, consider the shape functional:

$$J_T(\Omega) = \int_{T\cap\Omega} f(\boldsymbol{x})\,\mathrm{d}\boldsymbol{x}, \tag{77}$$

where, again, $f\in W^{1,1}(\mathbb{R}^d)$ and T is a fixed, bounded Lipschitz domain with piecewise smooth boundary. We seek to prove that (77) is Fréchet differentiable with respect to Ω keeping T fixed. In Section 4.4, T will correspond to an element in the mesh.

We start by introducing a smooth regularization ρ_ϵ of the characteristic function χ_T with $\epsilon > 0$, that satisfies the following properties:

$$\rho_\epsilon(\boldsymbol{x})\to\chi_T(\boldsymbol{x}) \quad \forall\,\boldsymbol{x}\notin\partial T, \quad \|\rho_\epsilon-\chi_T\|_{L^1(\mathbb{R}^d)}\to 0 \quad \text{as } \epsilon\to 0. \tag{78}$$

With this, we define

$$J_T^\epsilon(\Omega) = \int_\Omega \rho_\epsilon(\boldsymbol{x}) f(\boldsymbol{x}) \,\mathrm{d}\boldsymbol{x} \quad \Rightarrow \quad \lim_{\epsilon\to 0} J_T^\epsilon(\Omega) = \int_\Omega \chi_T(\boldsymbol{x}) f(\boldsymbol{x}) \,\mathrm{d}\boldsymbol{x} = J_T(\Omega). \tag{79}$$

The following assumption is crucial.

Assumption 2. Assume that $\partial\Omega \cap \partial T$ has vanishing $\mathbb{R}^{d-1}$ Lebesgue measure.

Under Assumption 2, we have that

$$\chi_{\partial\Omega}(\boldsymbol{x})\rho_\epsilon(\boldsymbol{x}) \to \chi_{\partial\Omega\cap T}(\boldsymbol{x}) \;\text{ for a.e. } \boldsymbol{x} \in \partial\Omega \qquad \text{as } \epsilon \to 0, \tag{80}$$

and also

$$\lim_{\epsilon\to 0} \int_{\partial\Omega} \rho_\epsilon(\boldsymbol{x}) g(\boldsymbol{x}) \,\mathrm{d}S(\boldsymbol{x}) = \int_{\partial\Omega\cap T} g(\boldsymbol{x}) \,\mathrm{d}S(\boldsymbol{x}) \quad \forall\, g \in L^1(\partial\Omega). \tag{81}$$

4.3.1 Fréchet differentiability on a cut subdomain

We first show the Fréchet differentiability of the shape functional for standard domain perturbations (analogous to Section 4.1). Throughout this subsection, we assume Ω is Lipschitz. We start with the following lemmas.

Lemma 4. *Given $f \in L^1(\mathbb{R}^d)$ and $\boldsymbol{U} \in [W^{1,\infty}(\mathbb{R}^d)]^d$ we have that*

$$\lim_{\|\boldsymbol{U}\|_{W^{1,\infty}}\to 0} \frac{\int_\Omega \left[f(\boldsymbol{\Phi}_{\boldsymbol{U}}(\boldsymbol{a}))\chi_T(\boldsymbol{\Phi}_{\boldsymbol{U}}(\boldsymbol{a})) - f(\boldsymbol{a})\chi_T(\boldsymbol{a})\right] G(\nabla_{\boldsymbol{a}}\boldsymbol{U}(\boldsymbol{a}))\mathrm{d}\boldsymbol{a}}{\|\boldsymbol{U}\|_{W^{1,\infty}}} = 0, \tag{82}$$

where $G\colon \mathbb{R}^{d\times d} \to \mathbb{R}$ is continuous and $|G(M)| \leqslant C|M|$ for all $M \in \mathbb{R}^{d\times d}$, for some bounded constant $C > 0$.

Proof. Since $\chi_T \in L^\infty(\mathbb{R}^d)$, then $f \cdot \chi_T \in L^1(\mathbb{R}^d)$. Thus, the result follows from Lemma 2. □

Lemma 5. *Given $f \in W^{1,1}(\mathbb{R}^d)$ and $\boldsymbol{U} \in [W^{1,\infty}(\mathbb{R}^d)]^d$ we have that*

$$\lim_{\|\boldsymbol{U}\|_{W^{1,\infty}}\to 0} \lim_{\epsilon\to 0} \frac{\int_\Omega f(\boldsymbol{\Phi}_{\boldsymbol{U}}(\boldsymbol{a}))\rho_\epsilon(\boldsymbol{\Phi}_{\boldsymbol{U}}(\boldsymbol{a})) - f(\boldsymbol{a})\rho_\epsilon(\boldsymbol{a})\mathrm{d}\boldsymbol{a} - \int_\Omega \nabla[f(\boldsymbol{a})\rho_\epsilon(\boldsymbol{a})]\cdot\boldsymbol{U}(\boldsymbol{a})\mathrm{d}\boldsymbol{a}}{\|\boldsymbol{U}\|_{W^{1,\infty}}} = 0, \tag{83}$$

provided Assumption 2 holds.

Proof. Let $\epsilon > 0$ be fixed and start by expanding the numerator in (83), i.e.

$$\begin{aligned} I_\epsilon(\boldsymbol{U}) &:= \int_\Omega f(\boldsymbol{\Phi}_{\boldsymbol{U}}(\boldsymbol{a}))\rho_\epsilon(\boldsymbol{\Phi}_{\boldsymbol{U}}(\boldsymbol{a})) - f(\boldsymbol{a})\rho_\epsilon(\boldsymbol{a})\mathrm{d}\boldsymbol{a} - \int_\Omega \nabla[f(\boldsymbol{a})\rho_\epsilon(\boldsymbol{a})]\cdot\boldsymbol{U}(\boldsymbol{a})\mathrm{d}\boldsymbol{a} \\ &= \int_\Omega \int_0^1 \left[\nabla\left[f(\boldsymbol{\Phi}_{s\boldsymbol{U}}(\boldsymbol{a}))\rho_\epsilon(\boldsymbol{\Phi}_{s\boldsymbol{U}}(\boldsymbol{a}))\right] - \nabla[f(\boldsymbol{a})\rho_\epsilon(\boldsymbol{a})]\right]\cdot\boldsymbol{U}(\boldsymbol{a})\mathrm{d}s\mathrm{d}\boldsymbol{a}, \end{aligned} \tag{84}$$

where we used the fundamental theorem of calculus. Expanding further, we get

$$\begin{aligned} I_\epsilon(\boldsymbol{U}) = &\int_\Omega \int_0^1 \left[\nabla\left[f(\boldsymbol{\Phi}_{s\boldsymbol{U}}(\boldsymbol{a}))\rho_\epsilon(\boldsymbol{\Phi}_{s\boldsymbol{U}}(\boldsymbol{a}))\right] - \nabla[f(\boldsymbol{\Phi}_{s\boldsymbol{U}}(\boldsymbol{a}))\rho_\epsilon(\boldsymbol{a})]\right]\cdot \boldsymbol{U}(\boldsymbol{a})\mathrm{d}s\mathrm{d}\boldsymbol{a} \\ &+ \int_\Omega \int_0^1 \left[\rho_\epsilon(\boldsymbol{a})\big(\nabla f(\boldsymbol{\Phi}_{s\boldsymbol{U}}(\boldsymbol{a})) - \nabla f(\boldsymbol{a})\big)\right]\cdot \boldsymbol{U}(\boldsymbol{a})\mathrm{d}s\mathrm{d}\boldsymbol{a} + \int_\Omega \int_0^1 \nabla\cdot\left[\rho_\epsilon(\boldsymbol{a})\big(f(\boldsymbol{\Phi}_{s\boldsymbol{U}}(\boldsymbol{a})) - f(\boldsymbol{a})\big)\boldsymbol{U}(\boldsymbol{a})\right]\mathrm{d}s\mathrm{d}\boldsymbol{a} \\ &- \int_\Omega \int_0^1 \rho_\epsilon(\boldsymbol{a})\nabla\cdot\left[\big(f(\boldsymbol{\Phi}_{s\boldsymbol{U}}(\boldsymbol{a})) - f(\boldsymbol{a})\big)\boldsymbol{U}(\boldsymbol{a})\right]\mathrm{d}s\mathrm{d}\boldsymbol{a} =: A_\epsilon^1 + A_\epsilon^2 + A_\epsilon^3 - A_\epsilon^4. \end{aligned} \tag{85}$$

Next, estimate A_ϵ^2. By the Lebesgue dominated convergence theorem and Fubini's theorem (using Proposition 2),

$$\begin{aligned} \lim_{\epsilon\to 0}\frac{|A_\epsilon^2|}{\|\boldsymbol{U}\|_{W^{1,\infty}}} &= \frac{1}{\|\boldsymbol{U}\|_{W^{1,\infty}}}\left|\int_\Omega \chi_T(\boldsymbol{a})\int_0^1 \big(\nabla f(\boldsymbol{\Phi}_{s\boldsymbol{U}}(\boldsymbol{a})) - \nabla f(\boldsymbol{a})\big)\cdot\boldsymbol{U}(\boldsymbol{a})\mathrm{d}s\mathrm{d}\boldsymbol{a}\right| \\ &\leqslant \frac{1}{\|\boldsymbol{U}\|_{W^{1,\infty}}}\int_0^1\int_{\Omega\cap T}\left|\nabla f(\boldsymbol{\Phi}_{s\boldsymbol{U}}(\boldsymbol{a})) - \nabla f(\boldsymbol{a})\right|\mathrm{d}\boldsymbol{a}\mathrm{d}s\cdot\|\boldsymbol{U}\|_{L^\infty} \leqslant \int_0^1\int_\Omega \left|\nabla f(\boldsymbol{\Phi}_{s\boldsymbol{U}}(\boldsymbol{a})) - \nabla f(\boldsymbol{a})\right|\mathrm{d}\boldsymbol{a}\mathrm{d}s. \end{aligned} \tag{86}$$

We then have

$$\lim_{\|\boldsymbol{U}\|_{W^{1,\infty}}\to 0}\lim_{\epsilon\to 0}\frac{|A_\epsilon^2|}{\|\boldsymbol{U}\|_{W^{1,\infty}}} = 0 \tag{87}$$

by a similar proof as in Lemma 3. For A_ϵ^3, we apply the divergence theorem:

$$\begin{aligned} \lim_{\epsilon\to 0} A_\epsilon^3 &= \lim_{\epsilon\to 0}\int_0^1\int_{\partial\Omega}\rho_\epsilon(\boldsymbol{a})\big(f(\boldsymbol{\Phi}_{s\boldsymbol{U}}(\boldsymbol{a})) - f(\boldsymbol{a})\big)\boldsymbol{U}(\boldsymbol{a})\cdot\boldsymbol{\nu}(\boldsymbol{a})\mathrm{d}S(\boldsymbol{a})\mathrm{d}s \\ &= \int_{\partial\Omega}\chi_T(\boldsymbol{a})\int_0^1\big(f(\boldsymbol{\Phi}_{s\boldsymbol{U}}(\boldsymbol{a})) - f(\boldsymbol{a})\big)\boldsymbol{U}(\boldsymbol{a})\cdot\boldsymbol{\nu}(\boldsymbol{a})\mathrm{d}s\mathrm{d}S(\boldsymbol{a}). \end{aligned} \tag{88}$$

Then,

$$\lim_{\|\boldsymbol{U}\|_{W^{1,\infty}}\to 0}\lim_{\epsilon\to 0}\frac{|A_\epsilon^3|}{\|\boldsymbol{U}\|_{W^{1,\infty}}} \leqslant \lim_{\|\boldsymbol{U}\|_{W^{1,\infty}}\to 0}\int_0^1\int_{\partial\Omega}\left|f(\boldsymbol{\Phi}_{s\boldsymbol{U}}(\boldsymbol{a})) - f(\boldsymbol{a})\right|\mathrm{d}S(\boldsymbol{a})\mathrm{d}s = 0 \tag{89}$$

by a similar argument as for A_ϵ^2 and using a trace theorem. As for A_ϵ^4, we have

$$\lim_{\epsilon\to 0} A_\epsilon^4 = \int_\Omega \chi_T(\boldsymbol{a})\int_0^1\nabla\cdot\left[\big(f(\boldsymbol{\Phi}_{s\boldsymbol{U}}(\boldsymbol{a})) - f(\boldsymbol{a})\big)\boldsymbol{U}(\boldsymbol{a})\right]\mathrm{d}s\mathrm{d}\boldsymbol{a}, \tag{90}$$

and so

$$\begin{aligned}\lim_{\|\boldsymbol{U}\|_{W^{1,\infty}}\to 0}\lim_{\epsilon\to 0}\frac{|A_\epsilon^4|}{\|\boldsymbol{U}\|_{W^{1,\infty}}} &\leqslant \lim_{\|\boldsymbol{U}\|_{W^{1,\infty}}\to 0}\frac{1}{\|\boldsymbol{U}\|_{W^{1,\infty}}}\int_0^1\int_{\Omega\cap T}\nabla\cdot\big[\big(f(\boldsymbol{\Phi}_{s\boldsymbol{U}}(\boldsymbol{a}))-f(\boldsymbol{a})\big)\boldsymbol{U}(\boldsymbol{a})\big]\mathrm{d}\boldsymbol{a}\mathrm{d}s\\ &\leqslant \lim_{\|\boldsymbol{U}\|_{W^{1,\infty}}\to 0}\int_0^1\int_{\Omega}\Big|\nabla\big(f(\boldsymbol{\Phi}_{s\boldsymbol{U}}(\boldsymbol{a}))-f(\boldsymbol{a})\big)\Big|\mathrm{d}\boldsymbol{a}\mathrm{d}s+\int_0^1\int_{\Omega}\big|f(\boldsymbol{\Phi}_{s\boldsymbol{U}}(\boldsymbol{a}))-f(\boldsymbol{a})\big|\mathrm{d}\boldsymbol{a}\mathrm{d}s\\ &\leqslant \gamma_1\|f-f_k\|_{W^{1,1}(\mathbb{R}^d)}\end{aligned}\tag{91}$$

for all $k \geqslant 1$ by a similar proof as in Lemma 3. Thus,

$$\lim_{\|\boldsymbol{U}\|_{W^{1,\infty}}\to 0}\lim_{\epsilon\to 0}\frac{|A_\epsilon^4|}{\|\boldsymbol{U}\|_{W^{1,\infty}}}=0.$$

Now, we expand A_ϵ^1:

$$\begin{aligned}A_\epsilon^1 &= \int_0^1\int_{\Omega}\boldsymbol{U}(\boldsymbol{a})\cdot\nabla f(\boldsymbol{\Phi}_{s\boldsymbol{U}}(\boldsymbol{a}))\big(\rho_\epsilon(\boldsymbol{\Phi}_{s\boldsymbol{U}}(\boldsymbol{a}))-\rho_\epsilon(\boldsymbol{a})\big)\mathrm{d}\boldsymbol{a}\mathrm{d}s\\ &+\int_0^1\int_{\Omega}\nabla\cdot\big[f(\boldsymbol{\Phi}_{s\boldsymbol{U}}(\boldsymbol{a}))\big(\rho_\epsilon(\boldsymbol{\Phi}_{s\boldsymbol{U}}(\boldsymbol{a}))-\rho_\epsilon(\boldsymbol{a})\big)\boldsymbol{U}(\boldsymbol{a})\big]\mathrm{d}\boldsymbol{a}\mathrm{d}s\\ &-\int_0^1\int_{\Omega}\big(\rho_\epsilon(\boldsymbol{\Phi}_{s\boldsymbol{U}}(\boldsymbol{a}))-\rho_\epsilon(\boldsymbol{a})\big)\nabla\cdot\big[f(\boldsymbol{\Phi}_{s\boldsymbol{U}}(\boldsymbol{a}))\boldsymbol{U}(\boldsymbol{a})\big]\mathrm{d}\boldsymbol{a}\mathrm{d}s=:B_\epsilon^1+B_\epsilon^2-B_\epsilon^3.\end{aligned}\tag{92}$$

By the Lebesgue dominated convergence theorem,

$$\lim_{\epsilon\to 0}\frac{|B_\epsilon^1|}{\|\boldsymbol{U}\|_{W^{1,\infty}}}\leqslant\int_0^1\int_{\Omega}|\nabla f(\boldsymbol{\Phi}_{s\boldsymbol{U}}(\boldsymbol{a}))|\big|\chi_T(\boldsymbol{\Phi}_{s\boldsymbol{U}}(\boldsymbol{a}))-\chi_T(\boldsymbol{a})\big|\mathrm{d}\boldsymbol{a}\mathrm{d}s.\tag{93}$$

For each fixed $\boldsymbol{U}$ and $s\in[0,1]$, let $E_s=\{\boldsymbol{a}\in\mathbb{R}^d \mid \big|\chi_T(\boldsymbol{\Phi}_{s\boldsymbol{U}}(\boldsymbol{a}))-\chi_T(\boldsymbol{a})\big|=1\}$, and note that $\big|\chi_T(\boldsymbol{\Phi}_{s\boldsymbol{U}}(\boldsymbol{a}))-\chi_T(\boldsymbol{a})\big|=0$ on $\mathbb{R}^d\backslash E_s$. Note that $\chi_T\circ\boldsymbol{\Phi}_{s\boldsymbol{U}}=\chi_{\widetilde{T}}$, i.e. is the characteristic function of $\widetilde{T}=\boldsymbol{\Phi}_{s\boldsymbol{U}}^{-1}(T)$.

A simple argument gives that $E_s\subset\widetilde{E}:=(T\backslash\widetilde{T})\cup(\widetilde{T}\backslash T)$. Set $\delta=s\|\boldsymbol{U}\|_{L^\infty}$. Clearly, $\mathrm{dist}(\boldsymbol{x},\partial T)\leqslant\delta$ for all $\boldsymbol{x}\in\widetilde{T}\backslash T$. Moreover, let $\boldsymbol{x}\in T\backslash\widetilde{T}$, so it has a pre-image $\boldsymbol{a}\notin T$ with $\boldsymbol{x}=\boldsymbol{\Phi}_{s\boldsymbol{U}}(\boldsymbol{a})$. Since $|\boldsymbol{x}-\boldsymbol{a}|\leqslant\delta$, and the line segment with endpoints $\boldsymbol{x},\boldsymbol{a}$ intersects ∂T, then $\mathrm{dist}(\boldsymbol{x},\partial T)\leqslant\delta$, which holds for all $\boldsymbol{x}\in T\backslash\widetilde{T}$. Therefore, by symmetry, we have $\mathrm{dist}(\boldsymbol{x},\partial T)\leqslant\delta$ for all $\boldsymbol{x}\in\widetilde{E}$.

Let ω_T be the signed distance function to ∂T that is negative inside T. Since ∂T is Lipschitz and piecewise smooth, the level sets $\{\omega_T=c\}$ are Lipschitz and piecewise smooth for all $|c|$ sufficiently small. Clearly,

$$\widetilde{E}\subset\widetilde{S}_\delta:=\{\omega_T\geqslant-\delta\}\cap\{\omega_T\leqslant\delta\}\equiv\{\omega_T\geqslant-\delta\}\backslash\{\omega_T>\delta\}.$$

Since the level sets are Lipschitz and piecewise smooth, one can show that $|\widetilde{S}_\delta|\leqslant\delta C_0$, where C_0 is a bounded constant depending on the perimeter of ∂T. Indeed, by the monotone convergence theorem, $\chi_{\widetilde{S}_\delta}\to\chi_{\partial T}$ as $\|\boldsymbol{U}\|_{W^{1,\infty}}\to 0$.

Returning to (93), we find that

$$\begin{aligned}\lim_{\epsilon\to 0}\frac{|B_\epsilon^1|}{\|\boldsymbol{U}\|_{W^{1,\infty}}} &\leqslant \gamma_2\|f-f_k\|_{W^{1,1}} + \max_{0\leqslant s\leqslant 1}\|\nabla f_k\circ\boldsymbol{\Phi}_{sU}\|_{L^\infty}\int_0^1\int_{E_s}1\mathrm{d}\boldsymbol{a}\mathrm{d}s \\ &\leqslant \gamma_2\|f-f_k\|_{W^{1,1}} + L_k\int_0^1\int_{\widetilde{S}_\delta}1\mathrm{d}\boldsymbol{a}\mathrm{d}s \leqslant \gamma_2\|f-f_k\|_{W^{1,1}} + L_kC_0\|\boldsymbol{U}\|_{L^\infty}.\end{aligned} \tag{94}$$

As before, we get

$$\lim_{\|\boldsymbol{U}\|_{W^{1,\infty}}\to 0}\lim_{\epsilon\to 0}\frac{|B_\epsilon^1|}{\|\boldsymbol{U}\|_{W^{1,\infty}}} = 0, \qquad \lim_{\|\boldsymbol{U}\|_{W^{1,\infty}}\to 0}\lim_{\epsilon\to 0}\frac{|B_\epsilon^3|}{\|\boldsymbol{U}\|_{W^{1,\infty}}} = 0,$$

where the B_ϵ^3 term follows similarly.

For B_ϵ^2, we have by the Divergence thm. and the Lebesgue dominated convergence thm.,

$$\lim_{\epsilon\to 0}\frac{|B_\epsilon^2|}{\|\boldsymbol{U}\|_{W^{1,\infty}}} \leqslant \int_0^1\int_{\partial\Omega}|f(\boldsymbol{\Phi}_{sU}(\boldsymbol{a}))|\big|\chi_T(\boldsymbol{\Phi}_{sU}(\boldsymbol{a})) - \chi_T(\boldsymbol{a})\big|\mathrm{d}S(\boldsymbol{a})\mathrm{d}s. \tag{95}$$

Similar to (94), we get

$$\begin{aligned}\lim_{\epsilon\to 0}\frac{|B_\epsilon^2|}{\|\boldsymbol{U}\|_{W^{1,\infty}}} &\leqslant \gamma_3\|f-f_k\|_{W^{1,1}} + \max_{0\leqslant s\leqslant 1}\||\nabla f_k\circ\boldsymbol{\Phi}_{sU}\|_{L^\infty}\int_0^1\int_{E_s\cap\partial\Omega}1\mathrm{d}S(\boldsymbol{a})\mathrm{d}s \\ &\leqslant \gamma_3\|f-f_k\|_{W^{1,1}} + L_k\int_0^1\int_{\widetilde{S}_\delta\cap\partial\Omega}1\mathrm{d}S(\boldsymbol{a})\mathrm{d}s,\end{aligned} \tag{96}$$

and note that, by the monotone convergence theorem, $\chi_{\widetilde{S}_\delta\cap\partial\Omega}\to\chi_{\partial T\cap\partial\Omega}$ as $\|\boldsymbol{U}\|_{W^{1,\infty}}\to 0$, which yields

$$\lim_{\|\boldsymbol{U}\|_{W^{1,\infty}}\to 0}\lim_{\epsilon\to 0}\frac{|B_\epsilon^2|}{\|\boldsymbol{U}\|_{W^{1,\infty}}} \leqslant \gamma_3\|f-f_k\|_{W^{1,1}} + L_k|\partial T\cap\partial\Omega|_{d-1}, \tag{97}$$

where $|\partial T\cap\partial\Omega|_{d-1}$ is the $\mathbb{R}^{d-1}$ Lebesgue measure of $\partial T\cap\partial\Omega$. Invoking Assumption 2, and taking the limit in k, we obtain

$$\lim_{\|\boldsymbol{U}\|_{W^{1,\infty}}\to 0}\lim_{\epsilon\to 0}\frac{|B_\epsilon^2|}{\|\boldsymbol{U}\|_{W^{1,\infty}}} = 0.$$

The proof of (83) is complete. □

Theorem 6. *Given the shape functional $J_T(\Omega) := \int_{\Omega\cap T} f(\boldsymbol{x})\mathrm{d}\boldsymbol{x}$ with $f\in W^{1,1}(\mathbb{R}^d)$ we have that $J_T(\Omega)$ is shape differentiable at Ω (in the sense of Definition 1) with Fréchet derivative $J_T'(\Omega)(\boldsymbol{U}) = \int_{\partial\Omega\cap T} f(\boldsymbol{a})\boldsymbol{U}(\boldsymbol{a})\cdot\boldsymbol{\nu}(\boldsymbol{a})\mathrm{d}S(\boldsymbol{a})$ for all $\boldsymbol{U}\in[W^{1,\infty}(\mathbb{R}^d)]^d$, provided Assumption 2 holds.*

Proof. Set $A_T(\boldsymbol{U}) := J_T'(\Omega)(\boldsymbol{U})$, let $\epsilon > 0$ be fixed, and define $A_T^\epsilon(\boldsymbol{U}) = \int_{\partial\Omega}\rho_\epsilon(\boldsymbol{a})f(\boldsymbol{a})\boldsymbol{U}(\boldsymbol{a})\cdot\boldsymbol{\nu}(\boldsymbol{a})\mathrm{d}S(\boldsymbol{a})$, where $A_T^\epsilon(\boldsymbol{U})\to A_T(\boldsymbol{U})$ by (81). Using (39), we have

$$\begin{aligned} J_T^\epsilon(\Omega_U) - J_T^\epsilon(\Omega) &= \int_\Omega \rho_\epsilon(\boldsymbol{\Phi}_U(\boldsymbol{a}))f(\boldsymbol{\Phi}_U(\boldsymbol{a}))\det(I+\nabla_{\boldsymbol{a}}\boldsymbol{U}(\boldsymbol{a}))\mathrm{d}\boldsymbol{a} - \int_\Omega \rho_\epsilon(\boldsymbol{a})f(\boldsymbol{a})\mathrm{d}\boldsymbol{a} \\ &= \int_\Omega \rho_\epsilon(\boldsymbol{\Phi}_U(\boldsymbol{a}))f(\boldsymbol{\Phi}_U(\boldsymbol{a})) - \rho_\epsilon(\boldsymbol{a})f(\boldsymbol{a})\mathrm{d}\boldsymbol{a} + \int_\Omega \rho_\epsilon(\boldsymbol{\Phi}_U(\boldsymbol{a}))f(\boldsymbol{\Phi}_U(\boldsymbol{a}))\mathrm{tr}(\nabla_{\boldsymbol{a}}\boldsymbol{U}(\boldsymbol{a}))\mathrm{d}\boldsymbol{a} \\ &\quad + \int_\Omega \rho_\epsilon(\boldsymbol{\Phi}_U(\boldsymbol{a}))f(\boldsymbol{\Phi}_U(\boldsymbol{a}))O(|\nabla_{\boldsymbol{a}}\boldsymbol{U}(\boldsymbol{a})|^2)\mathrm{d}\boldsymbol{a}. \end{aligned} \tag{98}$$

Continuing, we get

$$\begin{aligned} J_T^\epsilon(\Omega_U) - J_T^\epsilon(\Omega) &= \int_\Omega \rho_\epsilon(\boldsymbol{\Phi}_U(\boldsymbol{a}))f(\boldsymbol{\Phi}_U(\boldsymbol{a})) - \rho_\epsilon(\boldsymbol{a})f(\boldsymbol{a})\mathrm{d}\boldsymbol{a} - \int_\Omega \nabla_{\boldsymbol{a}}\big(\rho_\epsilon(\boldsymbol{a})f(\boldsymbol{a})\big)\cdot\boldsymbol{U}(\boldsymbol{a})\mathrm{d}\boldsymbol{a} \\ &\quad + \int_\Omega \big[\rho_\epsilon(\boldsymbol{\Phi}_U(\boldsymbol{a}))f(\boldsymbol{\Phi}_U(\boldsymbol{a})) - \rho_\epsilon(\boldsymbol{a})f(\boldsymbol{a})\big]\nabla_{\boldsymbol{a}}\cdot\boldsymbol{U}(\boldsymbol{a})\mathrm{d}\boldsymbol{a} \\ &\quad + \int_\Omega \big[\rho_\epsilon(\boldsymbol{a})f(\boldsymbol{a})\nabla_{\boldsymbol{a}}\cdot\boldsymbol{U}(\boldsymbol{a}) + \nabla_{\boldsymbol{a}}\big(\rho_\epsilon(\boldsymbol{a})f(\boldsymbol{a})\big)\cdot\boldsymbol{U}(\boldsymbol{a})\big]\mathrm{d}\boldsymbol{a} \\ &\quad + \int_\Omega \rho_\epsilon(\boldsymbol{\Phi}_U(\boldsymbol{a}))f(\boldsymbol{\Phi}_U(\boldsymbol{a}))O(|\nabla_{\boldsymbol{a}}\boldsymbol{U}(\boldsymbol{a})|^2)\mathrm{d}\boldsymbol{a}. \end{aligned} \tag{99}$$

By Gauss' divergence theorem, we arrive at

$$\begin{aligned} J_T^\epsilon(\Omega_U) - J_T^\epsilon(\Omega) - A_T^\epsilon(\boldsymbol{U}) &= \int_\Omega \rho_\epsilon(\boldsymbol{\Phi}_U(\boldsymbol{a}))f(\boldsymbol{\Phi}_U(\boldsymbol{a})) - \rho_\epsilon(\boldsymbol{a})f(\boldsymbol{a})\mathrm{d}\boldsymbol{a} - \int_\Omega \nabla_{\boldsymbol{a}}\big(\rho_\epsilon(\boldsymbol{a})f(\boldsymbol{a})\big)\cdot\boldsymbol{U}(\boldsymbol{a})\mathrm{d}\boldsymbol{a} \\ &\quad + \int_\Omega \big[\rho_\epsilon(\boldsymbol{\Phi}_U(\boldsymbol{a}))f(\boldsymbol{\Phi}_U(\boldsymbol{a})) - \rho_\epsilon(\boldsymbol{a})f(\boldsymbol{a})\big]\nabla_{\boldsymbol{a}}\cdot\boldsymbol{U}(\boldsymbol{a})\mathrm{d}\boldsymbol{a} \\ &\quad + \int_\Omega \rho_\epsilon(\boldsymbol{\Phi}_U(\boldsymbol{a}))f(\boldsymbol{\Phi}_U(\boldsymbol{a}))O(|\nabla_{\boldsymbol{a}}\boldsymbol{U}(\boldsymbol{a})|^2)\mathrm{d}\boldsymbol{a}. \end{aligned} \tag{100}$$

Then, by Lemmas 4 and 5, we find that

$$\lim_{\|\boldsymbol{U}\|_{W^{1,\infty}}\to 0}\frac{J_T(\Omega_U) - J_T(\Omega) - J_T'(\Omega)(\boldsymbol{U})}{\|\boldsymbol{U}\|_{W^{1,\infty}}} = \lim_{\|\boldsymbol{U}\|_{W^{1,\infty}}\to 0}\lim_{\epsilon\to 0}\frac{J_T^\epsilon(\Omega_U) - J_T^\epsilon(\Omega) - A_T^\epsilon(\boldsymbol{U})}{\|\boldsymbol{U}\|_{W^{1,\infty}}} = 0, \tag{101}$$

which proves the assertion. □

4.3.2 Level set Fréchet differentiability on a cut subdomain

We now prove the cut version of Theorem 5.

Theorem 7. *Adopt the hypothesis of Theorem 6 with the additional regularity that $f \in L^p(\mathbb{R}^d)$ for some $p > 2$. Assume $\phi \in W^{2,\infty}(\mathbb{R}^d)$ and that it satisfies Definition 2 for some positive constants c_0, δ_0. Let $\Omega(\phi+\eta)$ be the sub-zero level set of $\phi+\eta$. Then, $J_T(\Omega)$ is level set shape differentiable at Ω (in the sense of Definition 3) with Fréchet derivative $J_T'(\Omega)(\eta) = \int_{\partial\Omega\cap T} f(\boldsymbol{a})\big(-\eta(\boldsymbol{a})|\nabla\phi(\boldsymbol{a})|^{-1}\big)\mathrm{d}\boldsymbol{a}$ for all $\eta \in [W^{2,\infty}(\mathbb{R}^d)]^d$.*

Proof. First note that $\Omega(\phi+\eta) = \Omega_1 = \boldsymbol{\Phi}_1(\Omega_0) \equiv \widetilde{\boldsymbol{\Phi}}(\Omega)$ and $\Omega(\phi) = \Omega_0 \equiv \Omega$. In addition,

$$J_T'(\Omega(\phi))(\eta) = \int_{\partial\Omega(\phi)\cap T} f(\boldsymbol{a})\left(-\frac{\eta(\boldsymbol{a})}{|\nabla\phi(\boldsymbol{a})|}\right)\mathrm{d}\boldsymbol{a} = \int_{\partial\Omega\cap T} f(\boldsymbol{a})\boldsymbol{V}_\eta(\boldsymbol{a})\cdot\boldsymbol{\nu}\ \mathrm{d}\boldsymbol{a} = J_T'(\Omega)(\boldsymbol{V}_\eta),$$

where $\boldsymbol{V}_\eta$ is given by (57). Now, note that

$$\begin{aligned} J_T(\Omega(\phi+\eta)) &= \int_{\widetilde{\boldsymbol{\Phi}}(\Omega)\cap T} f(\boldsymbol{x})\mathrm{d}\boldsymbol{x} - \int_{\boldsymbol{\Phi}_\eta(\Omega)\cap T} f(\boldsymbol{x})\mathrm{d}\boldsymbol{x} + \int_{\boldsymbol{\Phi}_\eta(\Omega)\cap T} f(\boldsymbol{x})\mathrm{d}\boldsymbol{x} \\ &= \lim_{\epsilon\to 0}\int_{\widetilde{\boldsymbol{\Phi}}(\Omega)} f(\boldsymbol{x})\rho_\epsilon(\boldsymbol{x})\mathrm{d}\boldsymbol{x} - \int_{\boldsymbol{\Phi}_\eta(\Omega)} f(\boldsymbol{x})\rho_\epsilon(\boldsymbol{x})\mathrm{d}\boldsymbol{x} + J_T(\Omega_{\boldsymbol{V}_\eta}) \\ &= \lim_{\epsilon\to 0} \underbrace{\int_\Omega f(\widetilde{\boldsymbol{\Phi}}(\boldsymbol{a}))\rho_\epsilon(\widetilde{\boldsymbol{\Phi}}(\boldsymbol{a}))\det(\nabla_{\boldsymbol{a}}\widetilde{\boldsymbol{\Phi}}(\boldsymbol{a}))\mathrm{d}\boldsymbol{a} - \int_\Omega f(\boldsymbol{\Phi}_\eta(\boldsymbol{a}))\rho_\epsilon(\boldsymbol{\Phi}_\eta(\boldsymbol{a}))\det(\nabla_{\boldsymbol{a}}\boldsymbol{\Phi}_\eta(\boldsymbol{a}))\mathrm{d}\boldsymbol{a}}_{=Z_\epsilon} + J_T(\Omega_{\boldsymbol{V}_\eta}). \end{aligned} \tag{102}$$

Next, we split the Z_ϵ term as $Z_\epsilon = Q_\epsilon^1 + Q_\epsilon^2$, where

$$\begin{aligned} Q_\epsilon^1 &= \int_\Omega \Big(f(\widetilde{\boldsymbol{\Phi}}(\boldsymbol{a})) - f(\boldsymbol{\Phi}_\eta(\boldsymbol{a}))\Big)\rho_\epsilon(\widetilde{\boldsymbol{\Phi}}(\boldsymbol{a}))\det(\nabla_{\boldsymbol{a}}\widetilde{\boldsymbol{\Phi}}(\boldsymbol{a}))\mathrm{d}\boldsymbol{a} \\ &\quad + \int_\Omega f(\boldsymbol{\Phi}_\eta(\boldsymbol{a}))\rho_\epsilon(\boldsymbol{\Phi}_\eta(\boldsymbol{a}))\Big(\det(\nabla_{\boldsymbol{a}}\widetilde{\boldsymbol{\Phi}}(\boldsymbol{a})) - \det(\nabla_{\boldsymbol{a}}\boldsymbol{\Phi}_\eta(\boldsymbol{a}))\Big)\mathrm{d}\boldsymbol{a}, \\ Q_\epsilon^2 &= \int_\Omega \Big(\rho_\epsilon(\widetilde{\boldsymbol{\Phi}}(\boldsymbol{a})) - \rho_\epsilon(\boldsymbol{\Phi}_\eta(\boldsymbol{a}))\Big)f(\boldsymbol{\Phi}_\eta(\boldsymbol{a}))\det(\nabla_{\boldsymbol{a}}\widetilde{\boldsymbol{\Phi}}(\boldsymbol{a}))\mathrm{d}\boldsymbol{a}. \end{aligned} \tag{103}$$

Estimating Q_ϵ^1 is similar to (74), i.e. we have

$$\lim_{\epsilon\to 0}|Q_\epsilon^1| \leqslant C\|f\|_{W^{1,1}(\mathbb{R}^d)}\|\nabla\eta\|_{L^\infty}^2 + C\|f\|_{L^1(\mathbb{R}^d)}\Big(\|\eta\|_{W^{2,\infty}}^2 + \|\phi_k\|_{W^{3,\infty}}\|\eta\|_{L^\infty}^2 + \|\phi_k-\phi\|_{W^{2,\infty}}\|\eta\|_{L^\infty}\Big). \tag{104}$$

For Q_ϵ^2, we follow a similar argument to estimating (93). By the Lebesgue dominated convergence theorem,

$$\lim_{\epsilon\to 0}|Q_\epsilon^2| \leqslant C\int_\Omega |f(\boldsymbol{\Phi}_\eta(\boldsymbol{a}))|\Big|\chi_T(\widetilde{\boldsymbol{\Phi}}(\boldsymbol{a})) - \chi_T(\boldsymbol{\Phi}_\eta(\boldsymbol{a}))\Big|\mathrm{d}\boldsymbol{a}. \tag{105}$$

For each fixed η, let $E = \Big\{\boldsymbol{a}\in\mathbb{R}^d \mid \Big|\chi_T(\widetilde{\boldsymbol{\Phi}}(\boldsymbol{a})) - \chi_T(\boldsymbol{\Phi}_\eta(\boldsymbol{a}))\Big| = 1\Big\}$. Similar to the proof of (94), we find that $|E| \leqslant C\|\eta\|_{W^{1,\infty}}^2$ for a uniform constant C (recall Theorem 4). Therefore, with $p^{-1}+q^{-1}=1$, we find

$$\lim_{\epsilon\to 0}|Q_\epsilon^2| \leqslant C\|f\|_{L^p}\|\chi_E\|_{L^q} = C\|f\|_{L^p}|E|^{1/q} \leqslant C\|f\|_{L^p}|E|^{\gamma_0+1/2} \leqslant C\|f\|_{L^p}\|\eta\|_{W^{1,\infty}}^{1+2\gamma_0}, \tag{106}$$

where $\gamma_0 > 0$ and we used the extra regularity of f.

Therefore,

$$J_T(\Omega(\phi+\eta)) - J_T(\Omega(\phi)) - J_T'(\Omega(\phi))(\eta) = \lim_{\epsilon\to 0} Z_\epsilon + J_T(\Omega_{\boldsymbol{V}_\eta}) - J_T(\Omega) - J_T'(\Omega)(\boldsymbol{V}_\eta), \tag{107}$$

and since $\|\boldsymbol{V}_\eta\|_{W^{1,\infty}} \leqslant C_\eta\|\eta\|_{W^{1,\infty}}$ for all $k \geqslant 1$, we obtain

$$\begin{aligned} &\lim_{\|\eta\|_{W^{2,\infty}}\to 0} \frac{|J_T(\Omega(\phi+\eta)) - J_T(\Omega(\phi)) - J_T'(\Omega(\phi))(\eta)|}{\|\eta\|_{W^{2,\infty}}} \\ &\qquad \leqslant C\|\phi_k-\phi\|_{W^{2,\infty}} + C_\eta \lim_{\|\boldsymbol{V}_\eta\|_{W^{1,\infty}}\to 0} \frac{|J_T(\Omega_{\boldsymbol{V}_\eta}) - J_T(\Omega) - J_T'(\Omega)(\boldsymbol{V}_\eta)|}{\|\boldsymbol{V}_\eta\|_{W^{1,\infty}}} \leqslant C\|\phi_k-\phi\|_{W^{2,\infty}}, \end{aligned} \tag{108}$$

where we used Theorem 6. Taking $k\to\infty$ proves the result. □

4.4 Shape Fréchet differentiability over a mesh

We now consider piecewise defined functions over the mesh $\widehat{\mathcal{T}}_h$. In particular, on $\widehat{\mathcal{T}}_h$, define:

$$\mathcal{W}_h = \left\{ w_h \in L^1(\widehat{\mathfrak{D}}) \mid w_h|_T \in W^{1,1}(T) \quad \forall T \in \widehat{\mathcal{T}}_h \right\}, \tag{109}$$

with norm given by

$$\|w_h\|_{\mathcal{W}_h} := \|w_h\|_{L^1(\widehat{\mathfrak{D}})} + \sum_{T \in \widehat{\mathcal{T}}_h} \|\nabla w_h\|_{L^1(T)}. \tag{110}$$

By using the previous results, we can generalize Theorem 3 to allow for functions in $\mathcal{W}_h$. To this end, we need a global mesh version of Assumption 2.

Assumption 3. Assume that $\partial\Omega \cap \partial T$ has vanishing $\mathbb{R}^{d-1}$ Lebesgue measure for all $T \in \widehat{\mathcal{T}}_h$.

Theorem 8. *For the shape functional $J(\Omega) := \int_\Omega f_h(\boldsymbol{x})\mathrm{d}\boldsymbol{x}$ with $f_h \in \mathcal{W}_h$ we have that $J(\Omega)$ is shape differentiable at Ω (in the sense of Definition 1) with Fréchet derivative $J'(\Omega)(\boldsymbol{U}) = \int_{\partial\Omega} f_h(\boldsymbol{a})\boldsymbol{U}(\boldsymbol{a}) \cdot \boldsymbol{\nu}(\boldsymbol{a})\mathrm{d}\boldsymbol{a}$ for all $\boldsymbol{U} \in [W^{1,\infty}(\mathbb{R}^d)]^d$, provided Assumption 3 holds.*

Proof. First, note that $f_h|_T \in W^{1,1}(T)$ for all $T \in \widehat{\mathcal{T}}_h$. Let $f_T : \mathbb{R}^d \to \mathbb{R}$ be a bounded extension of $f_h|_T$ to $W^{1,1}(\mathbb{R}^d)$, for all $T \in \widehat{\mathcal{T}}_h$. Then,

$$J(\Omega_U) - J(\Omega) - J'(\Omega)(\boldsymbol{U}) = \sum_{T \in \widehat{\mathcal{T}}_h} J_T(\Omega_U) - J_T(\Omega) - J_T'(\Omega)(\boldsymbol{U}),$$

where

$$J_T(\Omega) = \int_{\Omega \cap T} f_T(\boldsymbol{a})\mathrm{d}\boldsymbol{a}, \quad J_T'(\Omega)(\boldsymbol{U}) = \int_{\partial\Omega \cap T} f_T(\boldsymbol{a})\boldsymbol{U}(\boldsymbol{a}) \cdot \boldsymbol{\nu}(\boldsymbol{a})\mathrm{d}\boldsymbol{a}. \tag{111}$$

For each term in the sum, one can apply Theorem 6. Since the sum is finite, we easily obtain the Fréchet shape differentiability of $J(\Omega)$. □

Next, we consider domains defined using the space $\mathcal{B}_h$ given in Section 3.1. Thus, let $\Omega(\phi_h)$ be the sub-zero level set of ϕ_h, where $\phi_h \in \mathcal{B}_h$ and satisfies Definition 2 for some positive constants c_0, δ_0. We will show that $J(\Omega(\phi_h))$ is level set shape Fréchet differentiable in the sense of Definition 3 with $\mathcal{X} = \mathcal{B}_h$.

Theorem 9. *Assume $\phi_h \in \mathcal{B}_h$ satisfies Definition 2 for some positive constants c_0, δ_0. For the shape functional $J(\Omega(\phi_h)) := \int_{\Omega(\phi_h)} f_h(\boldsymbol{x})\mathrm{d}\boldsymbol{x}$ with $f_h \in \mathcal{W}_h \cap L^p(\widehat{\mathfrak{D}})$ for some p>2, we have that $J(\Omega(\phi_h))$ is level set shape differentiable at $\Omega(\phi_h)$ (in the sense of Definition 3 with $\mathcal{X} = \mathcal{B}_h$) with Fréchet derivative $J'(\Omega(\phi_h))(\eta_h) = \int_{\partial\Omega(\phi_h)} f_h(\boldsymbol{a})\big(-\eta_h(\boldsymbol{a})|\nabla\phi_h(\boldsymbol{a})|^{-1}\big)\mathrm{d}\boldsymbol{a}$ for all $\eta_h \in \mathcal{B}_h$, provided Assumption 3 holds.*

Proof. We proceed similarly to the proof of Theorem 8. Let $f_T : \mathbb{R}^d \to \mathbb{R}$ be a bounded extension of $f_h|_T$ to $W^{1,1}(\mathbb{R}^d)$, for all $T \in \widehat{\mathcal{T}}_h$. Moreover, let $\phi_T : \mathbb{R}^d \to \mathbb{R}$ be a bounded extension of $\phi_h|_T$ to $W^{2,\infty}(\mathbb{R}^d)$, for all $T \in \widehat{\mathcal{T}}_h$; similarly, do a piecewise extension for η_h to $\{\eta_T\} \subset W^{2,\infty}(\mathbb{R}^d)$. See [52, Sec. VI.3.1] for details of the extension. Then,

$$J(\Omega(\phi_h + \eta_h)) - J(\Omega(\phi_h)) - J'(\Omega(\phi_h))(\eta_h) = \sum_{T \in \widehat{\mathcal{T}}_h} J_T(\Omega(\phi_T + \eta_T)) - J_T(\Omega(\phi_T)) - J_T'(\Omega(\phi_T))(\eta_T),$$

where

$$J_T(\Omega(\phi_T)) = \int_{\Omega(\phi_T) \cap T} f_T(\boldsymbol{a})\mathrm{d}\boldsymbol{a}, \quad J_T'(\Omega(\phi_T))(\eta_T) = \int_{\partial\Omega(\phi_T) \cap T} f_T(\boldsymbol{a})\left(-\frac{\eta_T}{|\nabla\phi_T(\boldsymbol{a})|}\right)\mathrm{d}\boldsymbol{a}. \tag{112}$$

For each term in the sum, one can apply Theorem 7. Since the sum is finite, we easily obtain the Fréchet shape differentiability of $J(\Omega(\phi_h))$. □

4.5 When the boundary intersects a facet

We now consider the case where Assumption 3 is violated. Suppose the violation happens on a single facet $F = \overline{T_+} \cap \overline{T_-}$ where $E := \partial\Omega \cap \partial T \subset F$ with $|E|_{d-1} > 0$. Since Ω is $C^{1,1}$, then $|\boldsymbol{\nu} \cdot \boldsymbol{n}| = 1$ on E where $\boldsymbol{n}$ is the outer normal of ∂T_+. Then, one can obtain the following modification of Theorem 8:

$$J'(\Omega)(\boldsymbol{U}) = \int_{\partial\Omega \setminus E} f_h \boldsymbol{U} \cdot \boldsymbol{\nu} \mathrm{d}S + \int_E \left[f_{h,+} \left(\frac{1 - \operatorname{sign}(\boldsymbol{U} \cdot \boldsymbol{n})}{2} \right) + f_{h,-} \left(\frac{1 + \operatorname{sgn}(\boldsymbol{U} \cdot \boldsymbol{n})}{2} \right) \right] \boldsymbol{U} \cdot \boldsymbol{n} \, \mathrm{d}S, \tag{113}$$

where $f_{h,\pm}$ is the restriction of f_h from $T_\pm$. Note that (113) is not a Fréchet derivative, or even a Gâteaux derivative, because (113) is not linear in $\boldsymbol{U}$; hence, we refer to (113) as the first variation of $J(\Omega)$. If f_h is continuous across the mesh, then (113) reduces the Fréchet derivative in Theorem 8.

The corresponding modification of Theorem 9 is given by

$$\begin{aligned} J'(\Omega(\phi_h))(\eta_h) = &- \int_{\partial\Omega \setminus E} f_h \frac{\eta_h}{|\nabla \phi_h|} \mathrm{d}S \\ &- \int_E \left[\frac{f_{h,+}}{|\nabla \phi_{h,+}|} \left(\frac{1 + \operatorname{sgn}(\eta_h (\nabla \phi_h \cdot \boldsymbol{n}))}{2} \right) + \frac{f_{h,-}}{|\nabla \phi_{h,-}|} \left(\frac{1 - \operatorname{sgn}(\eta_h (\nabla \phi_h \cdot \boldsymbol{n}))}{2} \right) \right] \eta_h \, \mathrm{d}S, \end{aligned} \tag{114}$$

where we have assumed that $\operatorname{sgn}(\nabla \phi_{h,+} \cdot \boldsymbol{n}) = \operatorname{sgn}(\nabla \phi_{h,-} \cdot \boldsymbol{n})$ on E with $\phi_{h,\pm}$ denoting the restriction of ϕ_h from $T_\pm$. If f_h *and* $\nabla \phi_h$ are continuous across the mesh, then (114) reduces the Fréchet derivative in Theorem 9.

We discuss the effects on the numerics of the domain boundary lying along a mesh facet in Section 6.3.

5 Unfitted shape optimization

We consider a discrete form of the optimization problem discussed in Section 2.2 using the unfitted formulation in (24). Furthermore, we develop a gradient-descent optimization method to find discrete minimizers using the level set shape derivative formulas derived earlier.

5.1 Admissible set

The domain Ω_h is parameterized by a level set function $\phi_h \in B_h$. Thus, in principle, we seek to minimize a shape functional $J(\Omega_h)$ over the set of admissible shapes

$$\widetilde{\mathcal{A}}_h = \left\{ \varphi_h \in B_h \mid c^{-1} \geqslant |\nabla \varphi_h| \geqslant c \right\} \tag{115}$$

for some suitable constant $c > 0$, where the inequality constraints are needed to ensure the domain does not degenerate. Unfortunately, $\widetilde{\mathcal{A}}_h$ is not a convex set.

Therefore, we define a localized admissible set, that is convex, in order to pose a well-defined minimization problem. Suppose we have a given domain Ω_h that is represented through the level set function $\phi_h \in \widetilde{\mathcal{A}}_h$. Next, define the convex set

$$C(\Sigma) = \{ \varphi_h \in B_h \mid |\nabla \varphi_h| \leqslant c/2, \ \varphi_h|_\Sigma = 0 \}, \tag{116}$$

where $\Sigma \subset \partial\widehat{\mathfrak{D}}$, which may be empty, is used to impose additional design constraints in our optimization (see Figure 4 for an example). Now, define the local admissible set $\mathcal{A}_h(\phi_h, \Sigma) = \{\phi_h\} + C(\Sigma)$, where ϕ_h is a given *reference* level set function, and note that any $\psi_h \in \mathcal{A}_h(\phi_h, \Sigma)$ satisfies $\psi_h = \phi_h + \varphi_h$, for some $\varphi_h \in C(\Sigma)$ and

$$|\nabla \phi_h + \nabla \varphi_h| \geqslant \big| |\nabla \phi_h| - |\nabla \varphi_h| \big| = |\nabla \phi_h| - |\nabla \varphi_h| \geqslant c - c/2 > c/2 > 0.$$

Ergo, any $\psi_h \in \mathcal{A}_h(\phi_h, \Sigma)$ parameterizes a well-defined domain as its sub-zero level set. In our computations, we iteratively update the convex set $\mathcal{A}_h(\cdot, \Sigma)$ in our gradient descent procedure (see Section 5.4).

In practice, we do not allow $|\nabla \phi_h|$ to become close to 0 during the optimization. In fact, we strive to maintain $|\nabla \phi_h| \approx 1$ or at least $|\nabla \phi_h| \geqslant \frac{1}{2}$. Then, the constraint in (116) corresponds to $|\nabla \varphi_h| \leqslant 1/4$. During the optimization, we periodically reinitialize ϕ_h so that it is close to a signed distance function having the same zero level set as before (see Section 5.4).

5.2 Discrete optimization problem

For any $\boldsymbol{v}_h \in V_h(\Omega_h(\phi_h))$, let $J(\phi_h; \boldsymbol{v}_h) \equiv J(\Omega_h(\phi_h); \boldsymbol{v}_h)$ be the shape (cost) functional in (5). For a given reference domain $\Omega_h(\widehat{\phi}_h)$, with reference level set function $\widehat{\phi}_h$, consider the following minimization problem

$$J(\phi_{h,\min}; \boldsymbol{u}_h(\phi_{h,\min})) = \min_{\substack{\phi_h \in \mathcal{A}_h(\widehat{\phi}_h, \Sigma), \\ \boldsymbol{u}_h \in V_h(\Omega_h(\phi_h))}} J(\phi_h; \boldsymbol{u}_h) \text{ subject to } \boldsymbol{u}_h \text{ solving (24) on } \Omega_h(\phi_h), \tag{117}$$

where $\boldsymbol{u}_h(\phi_h) \equiv \boldsymbol{u}_h(\Omega_h(\phi_h))$. Since B_h is finite dimensional, $\mathcal{A}_h(\widehat{\phi}_h, \Sigma)$ effectively enforces a bounded Lipschitz constant on the domains it contains; thus, $\mathcal{A}_h(\widehat{\phi}_h, \Sigma)$ has enough compactness to ensure existence of a minimizer (see [26]).

We rewrite the minimization problem using a Lagrangian to free the PDE-constraint, i.e. for any $\phi_h \in \mathcal{A}_h(\widehat{\phi}_h, \Sigma)$, define

$$L(\phi_h; \boldsymbol{v}_h, \boldsymbol{q}_h) := J(\phi_h; \boldsymbol{v}_h) - A_h(\Omega_h(\phi_h); \boldsymbol{v}_h, \boldsymbol{q}_h) + \chi_h(\Omega_h(\phi_h); \boldsymbol{q}_h) \quad \forall\, \boldsymbol{v}_h, \boldsymbol{q}_h \in B_h, \tag{118}$$

and note that by (24) the following property holds

$$J(\phi_h; \boldsymbol{u}_h(\phi_h)) = L(\phi_h; \boldsymbol{u}_h(\phi_h), \boldsymbol{q}_h) \quad \forall \boldsymbol{q}_h \in V_h(\Omega_h(\phi_h)) \tag{119}$$

for any $\phi_h \in \widetilde{\mathcal{A}}_h$. The Lagrangian framework allows us to characterize the minimizer in (117) as a saddle-point, i.e.

$$L(\bar{\phi}_h; \bar{\boldsymbol{u}}_h, \bar{\boldsymbol{p}}_h) = \min_{\substack{\phi_h \in \mathcal{A}_h(\widehat{\phi}_h, \Sigma), \\ \boldsymbol{u}_h \in V_h(\Omega_h(\phi_h))}} \max_{\boldsymbol{q}_h \in V_h(\Omega_h(\phi_h))} L(\phi_h; \boldsymbol{u}_h, \boldsymbol{q}_h) \tag{120}$$

for some $\bar{\phi}_h = \widehat{\phi}_h + \bar{q}_h$ with $\bar{q}_h \in C(\Sigma)$, $\bar{\boldsymbol{u}}_h \in V_h(\bar{\Omega}_h)$, and $\bar{\boldsymbol{p}}_h \in V_h(\bar{\Omega}_h)$, where $\bar{\Omega}_h \equiv \bar{\Omega}_h(\bar{\phi}_h)$. Since L is Fréchet differentiable, with $\delta_a L(\Omega; \boldsymbol{v}, \boldsymbol{q})(\cdot)$ denoting the Fréchet derivative with respect to the argument a, the following first order conditions must hold for $\bar{\boldsymbol{u}}_h$ and $\bar{\boldsymbol{p}}_h$:

$$\delta_{\boldsymbol{q}_h} L(\bar{\phi}_h; \bar{\boldsymbol{u}}_h, \bar{\boldsymbol{p}}_h)(\boldsymbol{z}_h) = 0, \quad \delta_{\boldsymbol{v}_h} L(\bar{\phi}_h; \bar{\boldsymbol{u}}_h, \bar{\boldsymbol{p}}_h)(\boldsymbol{w}_h) = 0 \quad \forall\, \boldsymbol{z}_h, \boldsymbol{w}_h \in V_h(\bar{\Omega}_h), \tag{121}$$

which implies that $\bar{\boldsymbol{u}}_h$ and $\bar{\boldsymbol{p}}_h$ solve the following variational problems

$$\begin{aligned} A_h\Big(\bar{\Omega}_h(\bar{\phi}_h); \bar{\boldsymbol{u}}_h, \boldsymbol{v}_h\Big) &= \chi_h\Big(\bar{\Omega}_h(\bar{\phi}_h); \boldsymbol{v}_h\Big) \quad \forall \boldsymbol{v}_h \in V_h(\bar{\Omega}_h), \\ A_h\Big(\bar{\Omega}_h(\bar{\phi}_h); \boldsymbol{w}_h, \bar{\boldsymbol{p}}_h\Big) &= \delta_{\boldsymbol{v}_h} J(\bar{\phi}_h; \bar{\boldsymbol{u}}_h)(\boldsymbol{w}_h) \quad \forall \boldsymbol{w}_h \in V_h(\bar{\Omega}_h). \end{aligned} \tag{122}$$

Thus, $\bar{\phi}_h = \phi_{h,\min}$, $\bar{\Omega}_h = \Omega_{h,\min}$, $\bar{\boldsymbol{u}}_h = \boldsymbol{u}_h(\phi_{h,\min})$ solves (24) on $\Omega_{h,\,\min}$, and $\bar{\boldsymbol{p}}_h = \boldsymbol{p}_h(\phi_{h,\min})$ solves an adjoint problem. In addition, we have the following first order condition for $\bar{\phi}_h$:

$$L'(\bar{\phi}_h; \bar{\boldsymbol{u}}_h, \bar{\boldsymbol{p}}_h)(r_h - \bar{q}_h) \geqslant 0 \quad \forall\, r_h \in C(\Sigma). \tag{123}$$

5.3 Reduced gradient

Note that, ultimately, we are after the derivative of the *reduced functional* $\mathcal{J}(\phi_h) := J(\phi_h; \boldsymbol{u}_h(\phi_h))$ in (119), i.e. we seek to compute the level set shape derivative $\mathcal{J}'(\phi_h)(\eta_h) \equiv J'(\phi_h; \boldsymbol{u}(\phi_h))(\eta_h)$, so that we can perform gradient based optimization. This is given by the Correa-Seeger theorem [20, pg. 427]:

$$\mathcal{J}'(\phi_h)(\eta_h) = L'(\phi_h; \bar{\boldsymbol{u}}_h(\phi_h), \bar{\boldsymbol{p}}_h(\phi_h))(\eta_h) \quad \forall\, \eta_h \in B_h \tag{124}$$

for any $\phi_h \in \widetilde{\mathcal{A}}_h$. In our case, because of (5), the problem is self-adjoint and $\bar{\boldsymbol{p}}_h = \bar{\boldsymbol{u}}_h$.

We now apply our results from Section 4.4 to compute (124). However, our formulas only consider bulk functionals (not boundary functionals). Thus, we restrict our problem by taking $\gamma_{\mathrm{N}} = 0, \Gamma_{\mathrm{D}} = \emptyset$, and $\boldsymbol{g}_{\mathrm{N}} \neq \boldsymbol{0}$ only within $\Sigma \subset \partial\widehat{\Omega}$. This allows us to avoid differentiating any boundary integrals (see discussion in Section 7). In addition, for convenience, we take $\boldsymbol{f} = \boldsymbol{0}$, which implies that $\chi_h(\Omega_h; \boldsymbol{v}_h)$ is independent of any shape perturbations in $C(\Sigma)$.

Evaluating the Fréchet derivatives, we obtain for all $\phi_h \in \widetilde{\mathcal{A}}_h$ that

$$\begin{aligned} &\chi_h'(\Omega_h(\phi_h); \boldsymbol{v}_h)(\eta_h) = 0, \quad J'(\Omega_h(\phi_h); \boldsymbol{v}_h)(\eta_h) = -a_0 \int_{\Gamma_h(\phi_h)} \frac{\eta_h}{|\nabla \phi_h|} \mathrm{d}S(\boldsymbol{x}), \\ &A_h'(\Omega_h(\phi_h); \boldsymbol{u}_h, \boldsymbol{v}_h)(\eta_h) = -\int_{\Gamma_h(\phi_h)} \left(2\mu \boldsymbol{\varepsilon}(\nabla \boldsymbol{u}_h) : \boldsymbol{\varepsilon}(\nabla \boldsymbol{v}_h) + \lambda(\nabla \cdot \boldsymbol{u}_h)(\nabla \cdot \boldsymbol{v}_h)\right) \frac{\eta_h}{|\nabla \phi_h|} \mathrm{d}S(\boldsymbol{x}) \end{aligned} \tag{125}$$

for all $\boldsymbol{u}_h, \boldsymbol{v}_h \in V_h(\Omega_h(\phi_h))$, and all $\eta_h \in B_h$; recall that $a_0 > 0$ is a volume penalty parameter. Note that the facet stabilization terms in (22) do not contribute anything because we take the facet patch selections to be fixed and independent of the perturbation η_h. Hence, since $\bar{\boldsymbol{p}}_h = \bar{\boldsymbol{u}}_h$, (124) reduces to

$$\mathcal{J}'(\phi_h)(\eta_h) = L'(\phi_h; \bar{\boldsymbol{u}}_h, \bar{\boldsymbol{p}}_h)(\eta_h) = \int_{\Gamma_h(\phi_h)} \left(2\mu |\boldsymbol{\varepsilon}(\nabla \bar{\boldsymbol{u}}_h)|^2 + \lambda(\nabla \cdot \bar{\boldsymbol{u}}_h)^2 - a_0\right) \frac{\eta_h}{|\nabla \phi_h|} \mathrm{d}S(\boldsymbol{x}). \tag{126}$$

Implementing (126) is straightforward within an unfitted finite element software, e.g. `ngsolve` [53], `ngsxfem` [54], provided Assumption 3 holds. Otherwise, we need to compute (114), which can be problematic. Fortunately, since ϕ_h is a piecewise polynomial, the set E in (114) must equal the entire facet F, which delivers some simplification. But (114) is still non-linear in the perturbation η_h. In our computations, we simply choose a side of F, either T_+ or T_-, which is automatically done by `ngsxfem` because the domain boundary is never allowed to fall exactly on a mesh facet. See Section 6.3 for more discussion on this, as well as Figure 3.

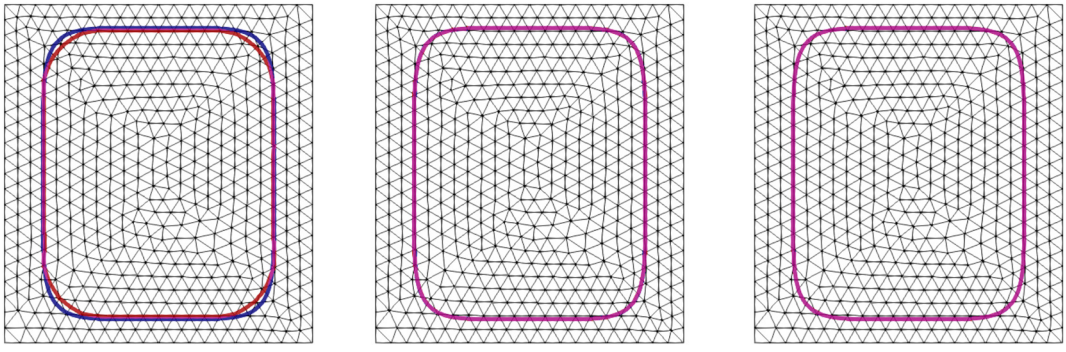

Figure 3: Superellipse ($p = 4$) shape optimization results. Background grid of the design domain is shown along with the exact interface in blue and the numerical interface in red. (a) Polynomial degree $k = 1$. (b) Polynomial degree $k = 2$. (c) Polynomial degree $k = 3$.

5.4 Shape optimization algorithm

Our algorithm is essentially gradient descent. Let $B(\omega_h, \eta_h)$ be a bilinear form defined for all ω_h, η_h in B_h; for example, we may take $B(\omega_h, \eta_h) = (\omega_h, \eta_h)_{H^1(\widehat{\mathfrak{D}})}$. Moreover, we introduce the following restricted finite element space $Q_h = \{\varphi_h \in B_h \mid \varphi_h|_\Sigma = 0\}$. Then, given a current domain $\Omega_h(\phi_h)$, we find a descent direction $\delta\phi_h \in Q_h$ that satisfies

$$B(\delta\phi_h, \eta_h) = -\mathcal{J}'(\phi_h)(\eta_h) \quad \forall\, \eta_h \in Q_h. \tag{127}$$

We then update ϕ_h by $\phi_h \leftarrow \phi_h + \alpha\delta\phi_h$, where $\alpha > 0$ is a step-size determined through a back-tracking line search. Note that the choice of the facet patches for stabilization stays fixed during the line search.

As mentioned earlier in Section 5.1, we want the level set function ϕ_h to satisfy $|\nabla\phi_h| \approx 1$ or at least $|\nabla\phi_h| \geqslant \frac{1}{2}$. To satisfy this requirement, we start with an initial level set function which is the signed distance function for our initial shape, hence $|\nabla\phi_h| = 1$ almost everywhere. The shape optimization algorithm however does not preserve this property and over many iterations we may no longer have $|\nabla\phi_h| \approx 1$. To remedy this, we reinitialize ϕ_h to that of a signed distance function after a set number of iterations.

Several methods for level set reinitialization on unstructured grids exist, such as the DRLSE algorithm [55], in which the reinitialization involves solving a fully explicit difference scheme. Other methods include [56], which use local projections and [57], which uses a fixed-point method.

In our algorithm, we compute the signed distance function directly by sampling the boundary, computing the signed distance using a sample from the entire mesh, and then computing a regularized least squares problem. One can also use the method in ref. [58].

6 Numerical results

We present some numerical tests to confirm the accuracy of our shape derivative formulation. Next, we solve a pure geometric shape optimization problem (no PDE constraint) using the algorithm in Section 5.4. Finally, we solve a shape optimization problem under the linear elasticity PDE constraint described in Section 2. All numerical tests were preformed using the NGSolve library [53] with the add-on package `ngsxfem` [54] for implementing the unfitted scheme. Note that the order of the geometry approximation matches the order of the finite element space used to solve a PDE constraint (when present).

6.1 First order accuracy test

For some fixed initial shape, given by ϕ_h, we define a perturbation η_h and compare our shape derivative formula with a finite difference approximation:

$$J'_{\text{FD}}(\phi_h)(\eta_h) = \frac{J(\phi_h + \epsilon\eta_h) - J(\phi_h)}{\epsilon}$$

for a sequence of decreasing ϵ. The design domain is defined to be $\widehat{\mathfrak{D}} := (0.0, 2.0) \times (0.0, 1.0)$ and the initial shape is $\Omega := \widehat{\mathfrak{D}} \setminus B_r(\boldsymbol{x}_0)$, where $B_r(\boldsymbol{x}_0)$ is the ball of radius r centered at $\boldsymbol{x}_0$ with $r = 0.2$ and $\boldsymbol{x}_0 = (0.3, 0.3)$. Here, the exact level set representation of Ω is $\phi(\boldsymbol{x}) = r - |\boldsymbol{x} - \boldsymbol{x}_0|$ and the exact perturbation is $\eta(\boldsymbol{x}) = \sin(3.3x + 2.5y)$. The cost functional $J(\Omega; \bar{\boldsymbol{u}}_h)$ is (5), where $\bar{\boldsymbol{u}}_h$ solves (24) on $\Omega(\phi_h)$. All elasticity and numerical parameters are the same as those used in Section 6.4. The exact shape derivative $J'_{\text{exact}}(\phi_h)(\eta_h)$ is given by (126).

We use degree $k = 1$ for B_h and set $\phi_h = I_h\phi$ and $\eta_h = I_h\eta$, where I_h is the standard nodal interpolant for B_h. In doing the comparison, we compute the following

$$\zeta(\epsilon) = \frac{\left|J'_{\text{exact}} - J'_{\text{FD}}\right|}{\epsilon}.$$

Table 1: Shape derivative test accuracy results.

ϵ	$J(\phi_h)$	$J(\phi_h + \epsilon\eta_h)$	J'_{exact}	J'_{FD}	ζ
1.0E-01	0.75860	0.95387	0.38283	1.95275	15.69922
1.0E-03	0.75860	0.75899	0.38283	0.38804	5.21949
1.0E-05	0.75860	0.75860	0.38283	0.38287	4.94585
1.0E-07	0.75860	0.75860	0.38283	0.38283	6.47544

Table 2: Translation test accuracy results.

t	$J(\phi_h(\cdot, t))$	$J(\phi_h(\cdot, t) + \epsilon\eta_h(\cdot))$	J'_{exact}	J'_{FD}	ζ
0.00	0.75860	0.75860	0.38283	0.38283	6.47544
0.05	0.74186	0.74186	0.13959	0.13959	12.51948
0.10	0.73253	0.73253	0.03503	0.03503	3.21555
0.15	0.72807	0.72807	0.02159	0.02159	4.34587
0.20	0.72670	0.72670	0.05205	0.05205	0.03602

The finite difference approximation is a first order accurate approximation of the exact formula, so if ζ remains bounded as $\epsilon \to 0$, then first order accuracy is confirmed; see Table 1. Note that taking ϵ smaller than 10^{-7} leads to a loss of accuracy because of round-off errors.

6.2 Translation test

This is a similar test as in the previous section, except we translate the hole with a given velocity. Specifically, we define $\Omega(t) := \widehat{\mathfrak{D}} \setminus B_r(\boldsymbol{x}(t))$, where $\boldsymbol{x}(t) = \boldsymbol{x}_0 + t\boldsymbol{v}$ with $\boldsymbol{x}_0 = (0.3, 0.3)$, $\boldsymbol{v} = (2.0, 1.0)$, $r = 0.2$, and set $\phi(\boldsymbol{x}, t)$ to be the signed distance function of $\Omega(t)$. We again choose the compliance functional with the same parameters, and set $\eta(\boldsymbol{x}) = \sin(3.3x + 2.5y)$ as our perturbation and fix $\epsilon = 10^{-7}$. We use degree $k = 1$ for B_h and set $\phi_h(\boldsymbol{x}, t) = I_h\phi(\boldsymbol{x}, t)$ and $\eta_h(\boldsymbol{x}) = I_h\eta(\boldsymbol{x})$. Table 2 gives the results.

6.3 Geometric problem

Consider the following purely geometric shape optimization problem. Let $u = u(x, y)$ be given by

$$u(x,y) = \frac{1}{p}\left(\frac{1}{\alpha}x^p + \frac{1}{\beta}y^p\right) \quad \Rightarrow \quad \nabla u = \left(\frac{1}{\alpha}x^{p-1}, \frac{1}{\beta}y^{p-1}\right), \quad |\nabla u|^2 = \left(\frac{x^{p-1}}{\alpha}\right)^2 + \left(\frac{y^{p-1}}{\beta}\right)^2 \tag{128}$$

for any $\alpha, \beta > 0$ and $p \geqslant 2$. Next, let $\lambda > 0$ and $A_0 > 0$ be given, and define the following shape functional:

$$J(\Omega) = \int_\Omega |\nabla u|^2 \, \mathrm{d}A - \lambda\big(|\Omega| - A_0\big), \tag{129}$$

and note that u does not depend on Ω. Standard shape differentiation yields

$$\delta J(\Omega; \boldsymbol{U}) = \int_{\partial\Omega} \big(|\nabla u|^2 - \lambda\big)\boldsymbol{U} \cdot \boldsymbol{\nu} \, \mathrm{d}S \tag{130}$$

for all smooth $\boldsymbol{U}$. For any critical point Ω^* of (129), we have $\delta J(\Omega^*; \boldsymbol{U}) = 0$ for all smooth $\boldsymbol{U}$, which yields the optimality conditions:

$$|\nabla u(x,y)|^2 = \lambda \quad \forall\, (x,y) \in \partial\Omega^*, \quad |\Omega^*| = A_0 \quad \Rightarrow \quad \left(\frac{x^{p-1}}{\alpha\sqrt{\lambda}}\right)^2 + \left(\frac{y^{p-1}}{\beta\sqrt{\lambda}}\right)^2 = 1, \tag{131}$$

which means $\partial\Omega^*$ is a superellipse depending on λ. Furthermore, the area constraint determines a unique relationship between λ and A_0 through the following relation from [59]:

$$4(\alpha\beta\lambda)^{\frac{1}{p-1}} \frac{\left(\Gamma\left(1+\frac{1}{2p-2}\right)\right)^2}{\Gamma\left(1+\frac{1}{p-1}\right)} = A_0, \tag{132}$$

where Γ represents the Gamma function.

In our numerical test, we take $\alpha = 1, \beta = 2, \lambda = 0.18$, and $p = 4$. The design domain is $\widehat{\mathfrak{D}} := (-1.0, 1.0) \times (-1.1, 1.1)$ and the initial guess for the optimal shape is a disk of radius 0.5 centered at the origin. We use $k = 1, 2, 3$ for B_h in the level set approximation ϕ_h. See Table 3 for a list of converged J and J' values for different mesh sizes.

The computed values of J' are the vector 2-norm of the coefficients of the basis representation of the linear form: $J'(\phi_h)(\eta_h) = \left((|\nabla u|^2 - \lambda)|\nabla\phi_h|^{-1}, \eta_h\right)_{\partial\Omega_h(\phi_h)}$. Since $p = 4$, the superellipse can be represented *exactly* by a discrete level set function using degree 6 piecewise polynomials. Thus, we computed the exact value of the cost at the minimizer, which is $J_{\text{exact}} = -0.3702425373188486$ and we confirmed that $|J'_{\text{exact}}| = 3.3 \cdot 10^{-18}$.

The `ngsxfem` add-on package to NGSolve uses an isoparametric mapping for implementing higher order unfitted schemes. But this is technically outside of our theory because we assume exact integration on the higher order interface without invoking an isoparametric map. On the other hand, `ngsxfem` provides an alternative method for integrating with higher order interfaces that uses subdivision of the underlying mesh. Essentially, with enough subdivision levels, one can get a sufficiently accurate approximation of the various integrals, which is the approach we use in this superellipse experiment.

Figure 3 shows plots of the numerical minimizers compared against the exact minimizer. We now discuss the practical issue of when the discrete boundary, $\partial\Omega_h$, lies along a mesh facet (recall Section 4.5). First, note that if $\partial\Omega_h$ has a non-trivial intersection with a facet F, then it must lie along the *entire* facet, because $\partial\Omega_h$ is represented by piecewise polynomials. Moreover, the `ngsxfem` package avoids these ambiguous situations by adding a small number, e.g. 10^{-14}, to the nodal values of the level set function ϕ_h that lie along the facet. In effect, this forces the derivative formula (114) to "choose a side."

Nevertheless, when the boundary does lie along a facet, the derivative of the cost is discontinuous at that facet. The practical effect on the optimization is that the numerical interface, $\partial\Omega_h$, can be "faceted." In Figure 3a, aside from the rounded corners where the numerical minimizer (red) deviates from the exact minimizer (blue), we see that the red interface (mostly) follows the mesh facets along the nearly straight portions of the interface. The exact interface, for the most part, does *not* lie along any mesh facets. This is particularly noticeable at the top of Figure 3a.

It is not surprising that the exact discrete minimizer has some mesh dependence. In these experiments, and others we have run, this effect is fairly mild. Moreover, this faceting effect is significantly reduced when using higher order methods, as Figure 3b and c indicates.

Table 3: Superellipse ($p = 4$) shape optimization results. The degree of B_h is k. The stopping criteria for each simulation was when the difference in J between successive iterations was less than 10^{-8}.

max h	$k=1$		$k=2$		$k=3$	
	$\lvert J - J_{\text{exact}}\rvert$	$\lvert J'\rvert$	$\lvert J - J_{\text{exact}}\rvert$	$\lvert J'\rvert$	$\lvert J - J_{\text{exact}}\rvert$	$\lvert J'\rvert$
0.1	1.1700e-03	1.7223e-02	3.6038E-05	1.5115E-06	1.9625E-07	9.0576E-08
0.05	7.3293E-04	5.0726E-03	4.8018E-06	3.7531E-07	9.5482E-09	4.3523E-08
0.025	1.7098E-04	2.2085E-03	2.0907E-07	1.2123E-07	1.9605E-10	1.6617E-08
0.0125	5.7855E-05	7.8292E-04	9.4514E-08	7.6382E-08	5.7451E-11	1.5158E-08

6.4 Shape optimization elasticity

We solve the shape optimization problem in (117), with the compliance shape functional (5), using our unfitted FEM framework. The material parameters are $\lambda = 0$, $\mu = 5$, and the area penalization is $a_0 = 0.3$. Moreover, we choose the facet stabilization parameter $\gamma_s = 2$ with layer thickness parameter $\delta = h$, and choose Nitsche stabilization parameters $\gamma_D = 10\mu$ and $\gamma_N = 0$.

We mimic the setup of [18] in order to compare our results. The design domain is $\widehat{\mathfrak{D}} := (0.0, 2.0) \times (0.0, 1.0)$ and the initial shape is depicted in Figure 4 (left), where the 10 (smaller) holes have a radius of 0.1, while the two "holes" centered at the top right and bottom right corners have radius 0.25. Furthermore, $\Gamma_D = \varnothing$ and $\widehat{\Gamma}_D$ consists of the line segment between (0.0, 0.0) and (0.0, 0.15) and a second line segment between (0.0, 1.0) and (0.0, 0.85). Also, $\boldsymbol{g}_N = (0.0, -1.0)$ on the line segment between (2.0, 0.4) and (2.0, 0.6), which is contained in $\widehat{\Gamma}_N$, and $\boldsymbol{g}_N = (0, 0)$ everywhere else. Figure 5 shows the initial domain shape for the optimization. We used a mesh size of $h = 0.02$.

Note that the level set function is constrained to *not* change along $\Sigma \subset \partial\widehat{\mathfrak{D}}$ as depicted in Figure 4 (right). This is to ensure the feasibility of the resulting shape. During the shape optimization process, we choose an initial step size of 0.4, and do a backtracking line search to determine the update of the shape.

The resulting optimal shapes for both piecewise linear and piecewise quadratic B_h are nearly identical (see Figure 6). The optimization history is given in Figure 7. The optimization for degree $k = 2$ used the isoparametric mapping approach in `ngsxfem` because the subdivision method would have been prohibitively expensive. Since the mesh size was $h = 0.02$, the isoparametric mapping was only a small perturbation from a linear triangle element. Nevertheless, this does induce a small error in our shape derivative, which introduces a small error when computing a descent direction. This is evidenced by the red curve in Figure 7a stopping at iteration index $\approx$340.

Figure 8 shows the accepted step size α versus iteration index. For degree $k = 1$, the step sizes do not get excessively small; toward the end of the optimization $\alpha = 0.025$. The same holds for degree $k = 2$, though it does prematurely stop at index $\approx$340 as discussed earlier.

We also performed a numerical optimization (not shown) with $\mu = 3.846 \cdot 10^3$ and $\lambda = 5.769 \cdot 10^3$ chosen to model a slightly incompressible material. The optimization performed similarly with reasonable step sizes and optimized shapes.

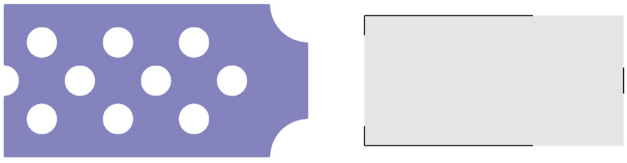

Figure 4: Left: initial shape for optimization algorithm. Right: level set function constraint set $\Sigma \subset \partial\widehat{\mathfrak{D}}$ denoted by solid lines.

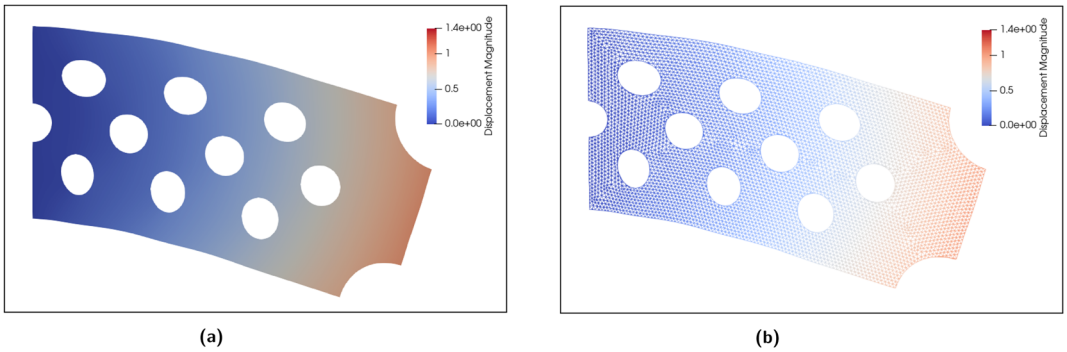

(a) (b)

Figure 5: Initial shape for the optimization algorithm. (a) The initial guess and an exaggerated displacement of the cantilever is shown. (b) Same initial shape, but with the mesh shown.

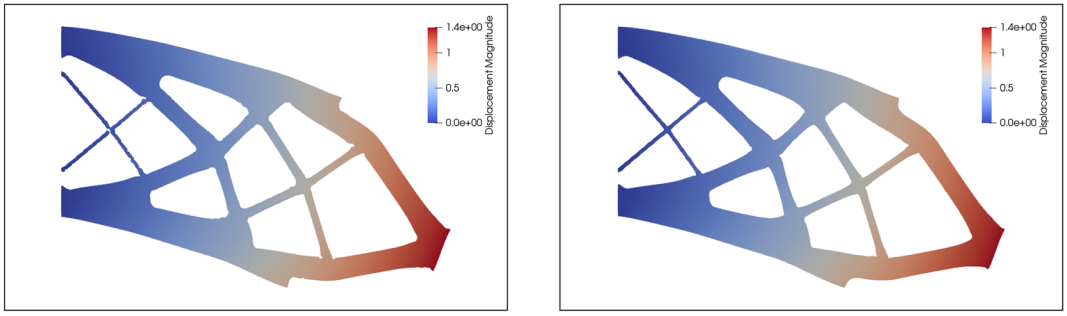

Figure 6: Resulting optimal shapes using degree $k = 1$ and $k = 2$ for B_h. (a) Optimal shape (exaggerated displacement) with degree $k = 1$. (b) Optimal shape (exaggerated displacement) with degree $k = 2$.

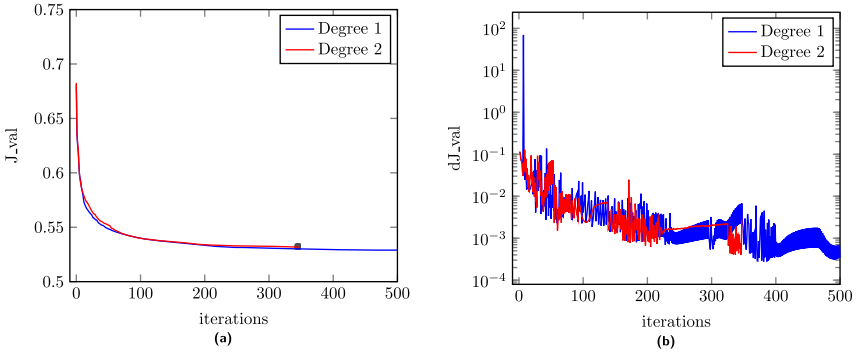

Figure 7: Optimization history. Blue indicates degree $k = 1$ for B_h; red indicates degree $k = 2$. (a) Cost J versus iteration index. (b) Norm of $|J'|$ versus iteration index.

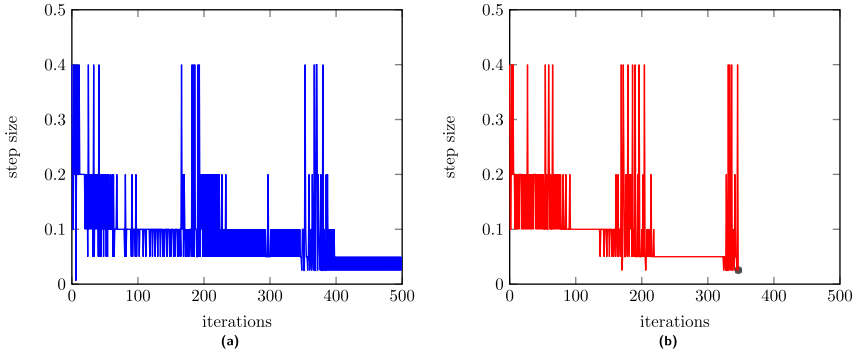

Figure 8: Accepted step size versus iteration index. The maximum step size allowed was $\alpha = 0.4$. (a) Degree $k = 1$ for B_h. (b) Degree $k = 2$ for B_h.

7 Conclusion

We presented a numerical shape optimization technique that takes advantage of unfitted finite element methods. We showed how to compute the exact discrete shape derivative of bulk shape functionals, under mild assumptions, and establish the Fréchet differentiability of discrete bulk shape functionals. This is done using both the perturbation of the identity approach, as well as direct perturbation of the level set representation of the domain. Our formulation allows for including a discrete PDE constraint and our discrete derivative mimics the shape derivative formula from the continuous problem. In other words, our method enjoys advantages of both the discretize-then-optimize and optimize-then-discretize philosophies.

We illustrated our method by considering the shape optimization of an elastic body. Specifically, we used a Lagrangian approach to deal with the linear elasticity PDE constraint. Furthermore, our level set based shape derivative approach allowed for *directly* optimizing the level set representation of the domain. No ad-hoc extension velocities were needed to update the level set function. Our numerical results demonstrated the effectiveness of our approach. For instance, the step sizes chosen by our gradient descent method are not excessively small, which can happen with some optimize-then-discretize approaches.

Our method can be easily applied to a two-phase material problem, such as an elastic body with a fixed shape but with two different material regions, Ω_1 and Ω_2, inside. In this case, the level set function marks one of the phases, say Ω_1, and the weak formulation involves a sum over the two sub-domains. As long as there is no boundary integral over $\partial\Omega_1 \cap \partial\Omega_2$ in the weak form, our methodology can be applied.

A point of future work is to extend our method to handle boundary functionals. Most likely, this will require some kind of regularization of the cost functional. Another area to investigate is the connection of our method to time-dependent problems, i.e. to extend our approach to solving PDEs in time-dependent geometries, as well as shape optimization with time-varying shape constraints.

Research ethics: Not applicable.
Informed consent: Not applicable.
Author contributions: All authors have accepted responsibility for the entire content of this manuscript and approved its submission.
Use of Large Language Models, AI and Machine Learning Tools: None declared.
Conflict of interest: The authors state no conflict of interest.
Research funding: National Science Foundation (NSF): DMS-2111474.
Data availability: Not applicable.

References

[1] J. Haslinger and R. A. E. Mäkinen, *Introduction to Shape Optimization: Theory, Approximation, and Computation*, vol. 7 of Advances in Design and Control, Philadelphia, PA, SIAM, 2003.
[2] A. Henrot and M. Pierre, *Shape Variation and Optimization*, vol. 28 of EMS Tracts in Mathematics, Zürich, European Mathematical Society (EMS), 2018.
[3] O. Pironneau, *Optimal Shape Design for Elliptic Systems*, Springer Series in Computational Physics, New York, NY, Springer-Verlag, 1984.
[4] S. Schmidt and V. H. Schulz, "A linear view on shape optimization," *SIAM J. Control Optim.*, vol. 61, no. 4, pp. 2358—2378, 2023.
[5] J. Sokolowski and J.-P. Zolésio, *Introduction to Shape Optimization*, Springer Series in Computational Mathematics, Springer-Verlag, 1992.
[6] S. W. Walker, *The Shapes of Things: A Practical Guide to Differential Geometry and the Shape Derivative*, vol. 28 of Advances in Design and Control, 1st ed. Philadelphia, PA, SIAM, 2015.
[7] M. Hinze, R. Pinnau, M. Ulbrich, and S. Ulbrich, *Optimization with PDE Constraints*, vol. 23 of Mathematical Modeling: Theory and Applications, New York, Springer, 2009.
[8] F. Tröltzsch, *Optimal Control of Partial Differential Equations*, Graduate Studies in Mathematics, Providence, RI, American Mathematical Society, 2010.
[9] M. D. Gunzburger and H. Kim, "Existence of an optimal solution of a shape control problem for the stationary Navier-Stokes equations," *SIAM J. Control Optim.*, vol. 36, no. 3, pp. 895—909, 1998.
[10] B. Mohammadi and O. Pironneau, *Applied Shape Optimization for Fluids*, Numerical Mathematics and Scientific Computation, New York, NY, The Clarendon Press Oxford University Press, 2001.
[11] O. Pironneau, "On optimum profiles in Stokes flow," *J. Fluid Mech.*, vol. 59, no. 1, pp. 117—128, 1973.
[12] O. Pironneau, "On optimum design in fluid mechanics," *J. Fluid Mech.*, vol. 64, no. 1, pp. 97—110, 1974.
[13] G. Doğan, P. Morin, and R. H. Nochetto, "A variational shape optimization approach for image segmentation with a Mumford—Shah functional," *SIAM J. Sci. Comput.*, vol. 30, no. 6, pp. 3028—3049, 2008.
[14] M. Hintermüller and W. Ring, "A second order shape optimization approach for image segmentation," *SIAM J. Appl. Math.*, vol. 64, no. 2, pp. 442—467, 2004.
[15] A. Laurain and S. W. Walker, "Droplet footprint control," *SIAM J. Control Optim.*, vol. 53, no. 2, pp. 771—799, 2015.

[16] S. W. Walker and E. E. Keaveny, "Analysis of shape optimization for magnetic microswimmers," *SIAM J. Control Optim.*, vol. 51, no. 4, pp. 3093—3126, 2013.
[17] S. W. Walker and M. J. Shelley, "Shape optimization of peristaltic pumping," *J. Comput. Phys.*, vol. 229, no. 4, pp. 1260—1291, 2010.
[18] E. Burman, D. Elfverson, P. Hansbo, M. G. Larson, and K. Larsson, "Shape optimization using the cut finite element method," *Comput. Methods Appl. Mech. Eng.*, vol. 328, pp. 242—261, 2018.
[19] D. Chenais, B. Rousselet, and R. Benedict, "Design sensitivity for arch structures with respect to midsurface shape under static loading," *J. Optim. Theor. Appl.*, vol. 58, no. 2, pp. 225—239, 1988.
[20] M. C. Delfour and J.-P. Zolésio, *Shapes and Geometries: Analysis, Differential Calculus, and Optimization*, vol. 4 of Advances in Design and Control, 2nd ed. Philadelphia, PA, SIAM, 2011.
[21] G. Iancu and E. Schnack, *Shape Optimization with FEM*, Vienna, Springer Vienna, 1992, pp. 411—430.
[22] M. Berggren, *A Unified Discrete—Continuous Sensitivity Analysis Method for Shape Optimization*, Dordrecht, Springer Netherlands, 2010, pp. 25—39.
[23] P. Gangl and M. H. Gfrerer, "A unified approach to shape and topological sensitivity analysis of discretized optimal design problems," *Appl. Math. Optim.*, vol. 88, no. 2, p. 46, 2023.
[24] R. Herzog and E. Loayza-Romero, "A discretize-then-optimize approach to pde-constrained shape optimization," *ESAIM: COCV*, vol. 30, p. 11, 2024.
[25] E. Laporte and P. L. Tallec, *Numerical Methods in Sensitivity Analysis and Shape Optimization*, Modeling and Simulation in Science, Boston, MA, Engineering and Technology, Birkhäuser, 2003.
[26] G. Allaire, C. Dapogny, and F. Jouve, "Chapter 1 — shape and topology optimization," in *Geometric Partial Differential Equations — Part II*, A. Bonito and R. H. Nochetto, Eds., vol. 22 of Handbook of Numerical Analysis, Amsterdam, Netherlands, Elsevier, 2021, pp. 1—132.
[27] N. Lachenmaier, D. Baumgärtner, H. P. Schiffer, and J. Kech, *Gradient-Based Optimization of a Radial Turbine Volute and a Downstream Bend Using Vertex Morphing*, vol. 2E: *Turbomachinery of Turbo Expo: Power for Land, Sea, and Air*, 2020.
[28] F. Mohebbi and M. Sellier, "Three-dimensional optimal shape design in heat transfer based on body-fitted grid generation," *Int. J. Comput. Methods Eng. Sci. Mech.*, vol. 14, no. 6, pp. 473—490, 2013.
[29] R. Bergmann, R. Herzog, E. Loayza-Romero, and K. Welker, "Shape optimization: what to do first, optimize or discretize?," *PAMM*, vol. 19, no. 1, p. e201900067, 2019.
[30] M. D. Gunzburger, *Perspectives in Flow Control and Optimization*, Philadelphia, PA, SIAM, 2003.
[31] P. Duysinx, L. Van Miegroet, T. Jacobs, and C. Fleury, "Generalized shape optimization using X-FEM and level set methods," in *IUTAM Symposium on Topological Design Optimization of Structures, Machines and Materials*, M. P. Bendsøe, N. Olhoff, and O. Sigmund, Eds., Dordrecht, Springer Netherlands, 2006, pp. 23—32.
[32] J. S. Dokken, S. W. Funke, A. Johansson, and S. Schmidt, "Shape optimization using the finite element method on multiple meshes with Nitsche coupling," *SIAM J. Sci. Comput.*, vol. 41, no. 3, pp. A1923—A1948, 2019.
[33] M. Berggren, "Shape calculus for fitted and unfitted discretizations: domain transformations vs. boundary-face dilations," *Commun. Optim. Theory*, vol. 2023, pp. 1—33, 2023.
[34] E. Burman, C. He, and M. G. Larson, "Comparison of shape derivatives using CutFEM for ill-posed Bernoulli free boundary problem," *J. Sci. Comput.*, vol. 88, no. 2, p. 35, 2021.
[35] E. G. Birgin, A. Laurain, R. Massambone, and A. G. Santana, "A shape-Newton approach to the problem of covering with identical balls," *SIAM J. Sci. Comput.*, vol. 44, no. 2, pp. A798—A824, 2022.
[36] E. G. Birgin, A. Laurain, and T. C. Menezes, "Sensitivity analysis and tailored design of minimization diagrams," *Math. Comput.*, vol. 92, no. 4, pp. 2715—2768, 2023.
[37] E. Burman, "Ghost penalty," *C. R. Math.*, vol. 348, no. 21, pp. 1217—1220, 2010.
[38] E. Burman, S. Claus, P. Hansbo, M. G. Larson, and A. Massing, "CutFEM: discretizing geometry and partial differential equations," *Int. J. Numer. Methods Eng.*, vol. 104, no. 7, pp. 472—501, 2014.
[39] E. Burman, P. Hansbo, M. G. Larson, and S. Zahedi, "Cut finite element methods for coupled bulk—surface problems," *Numer. Math.*, vol. 133, no. 2, pp. 203—231, 2016.
[40] A. Hansbo, P. Hansbo, and M. G. Larson, "A finite element method on composite grids based on Nitsche's method," *ESAIM: M2AN*, vol. 37, no. 3, pp. 495—514, 2003. Available at: https://doi.org/10.1051/m2an:2003039.
[41] C. Lehrenfeld and M. Olshanskii, "An Eulerian finite element method for PDEs in time-dependent domains," *ESAIM Math. Model. Numer. Anal.*, vol. 53, no. 2, pp. 585—614, 2019.
[42] P. Hansbo, M. G. Larson, and K. Larsson, "Cut finite element methods for linear elasticity problems," in *Geometrically Unfitted Finite Element Methods and Applications*, vol. 121 of Lecture Notes in Computational Science and Engineering, S. Bordas, E. Burman, M. Larson, and M. Olshanskii, Eds., New York, NY, Springer International Publishing, 2017, pp. 25—63.
[43] S. Osher and R. Fedkiw, *Level Set Methods and Dynamic Implicit Surfaces*, New York, NY, Springer-Verlag, 2003.
[44] S. A. Sethian, *Level Set Methods and Fast Marching Methods*, 2nd ed. New York, NY, Cambridge University Press, 1999.
[45] D. Baumgärtner, J. Wolf, R. Rossi, P. Dadvand, and R. Wüchner, "A robust algorithm for implicit description of immersed geometries within a background mesh," *Adv. Model. Simul. Eng. Sci.*, vol. 5, no. 1, p. 21, 2018.

[46] E. Burman and P. Hansbo, “Fictitious domain finite element methods using cut elements: II. A stabilized Nitsche method,” *Appl. Numer. Math.*, vol. 62, no. 4, pp. 328—341, 2012.
[47] S. C. Brenner and L. R. Scott, *The Mathematical Theory of Finite Element Methods*, vol. 15 of Texts in Applied Mathematics, 3rd ed. New York, NY, Springer, 2008.
[48] S. Gross, M. A. Olshanskii, and A. Reusken, “A trace finite element method for a class of coupled bulk-interface transport problems,” *ESAIM: M2AN*, vol. 49, no. 5, pp. 1303—1330, 2015.
[49] S. J. Osher and F. Santosa, “Level set methods for optimization problems involving geometry and constraints I. frequencies of a two-density inhomogeneous drum,” *J. Comput. Phys.*, vol. 171, no. 1, pp. 272—288, 2001.
[50] A. Laurain, “Analyzing smooth and singular domain perturbations in level set methods,” *SIAM J. Math. Anal.*, vol. 50, no. 4, pp. 4327—4370, 2018.
[51] J. K. Hale, *Ordinary Differential Equations*, *Dover Books on Mathematics*, Garden City, New York, Dover Publications, 1980.
[52] E. M. Stein, *Singular Integrals and Differentiability Properties of Functions (PMS-30)*, Princeton, NJ, Princeton University Press, 1970.
[53] J. Schöberl, “C++11 implementation of finite elements in NGSolve,” Institute for Analysis and Scientific Computing, Tech. Rep. ASC-2014-30, 2014.
[54] C. Lehrenfeld, F. Heimann, J. Preuss, and H. von Wahl, “ngsxfem: Add-on to NGSolve for geometrically unfitted finite element discretizations,” *J. Open Source Softw.*, vol. 6, no. 64, p. 3237, 2021.
[55] C. Li, C. Xu, C. Gui, and M. D. Fox, “Distance regularized level set evolution and its application to image segmentation,” *IEEE Trans. Image Process.*, vol. 19, no. 12, pp. 3243—3254, 2010.
[56] N. Parolini and E. Burman, “A local projection reinitialization procedure for the level set equation on unstructured grids,” École Polytechnique Fédérale de Lausanne, Tech. Rep. CMCS-REPORT-2007-004, 2007.
[57] C. Basting and D. Kuzmin, “A minimization-based finite element formulation for interface-preserving level set reinitialization,” *Computing*, vol. 95, no. 1, pp. 13—25, 2013.
[58] R. I. Saye, “High-order methods for computing distances to implicitly defined surfaces,” *Commun. Appl. Math. Comput. Sci.*, vol. 9, no. 1, pp. 107—141, 2014.
[59] A. Jaklič, A. Leonardis, and F. Solina, *Segmentation and Recovery of Superquadrics*, Computational Imaging and Vision, 1st ed. Dordrecht, Springer, 2010.